Korean J. Chem. Eng., 33(2), 351-387 (2016)
DOI: 10.1007/s11814-015-0296-3

pISSN: 0256-1115
eISSN: 1975-7220

INVITED REVIEW PAPER

Efficient thermal desalination technologies with renewable energy systems: A state-of-the-art review

Iman Janghorban Esfahani[‡], Jouan Rashidi[‡], Pouya Ifaei[‡], and ChangKyoo Yoo[†]

Department of Environmental Science and Engineering, College of Engineering, Center for Environmental Studies, Kyung Hee University, Seocheon-dong 1, Giheung-gu, Yongin-si, Gyeonggi-do 17104, Korea
(*Received 6 May 2015 • accepted 28 December 2015*)

Abstract−Due to the current fossil fuel crisis and associated adverse environmental impacts, renewable energy sources (RES) have drawn interest as alternatives to fossil fuels for powering water desalination systems. Over the last few decades the utility of renewable energy sources such as solar, geothermal, and wind to run desalination processes has been explored. However, the expansion of these technologies to larger scales is hampered by techno-economic and thermo-economic challenges. This paper reviews the state-of-the-art in the field of renewable energy-powered thermal desalination systems (RE-PTD) to compare their productivity and efficiency through thermodynamic, economic, and environmental analyses. We performed a comparative study using published data to classify RE-PTD systems technologies on the basis of the energy collection systems that they use. Among RE-PTD systems, solar energy powered-thermal desalination systems demonstrate high thermo-environ-economic efficiency to produce fresh water to meet various scales of demand.

Keywords: Renewable Energy, Desalination, Thermo-economic, Energy, Exergy

INTRODUCTION

Population growth and changing weather conditions have exacerbated shortages of freshwater in many countries [1]. Approximately 400 million people now live in areas where drinking water is scarce, and this number may grow to 4 billion by mid-century. Most of the earth's water has salinity of up to 10,000 ppm, whereas seawater normally has salinity in the range of 35,000-45,000 ppm total dissolved salts [2]. Desalination technologies have greatly improved in the past few decades in order to produce potable water with salinity of 500 ppm (according to the World Health Organization) and in special cases, up to 1,000 ppm. The two most widely used desalination techniques are membrane-based technologies such as reverse osmosis (RO), membrane distillation (MD) and electrodialysis (ED), and thermal-based technologies such as multi-effect distillation (MED) and multi-stage flash (MSF) desalination systems. Currently, thermal desalination processes account for more than 65% of the production capacity of the desalination industry [2-4].

Desalination is an energy-intensive process that requires expensive non-renewable fossil fuels, thereby contributing to global warming, air pollution, and environmental restrictions [5,6]. More sustainable energy sources such as renewable energies should be used to develop sustainable and environmentally friendly desalination systems. Selection of the most suitable renewable energy-powered desalination (RE-PD) technology depends on factors such as location of operation, amount of water production, size of the site, type of technology, and production costs related to the salinity of the feed water, remoteness, access to an electrical grid, and the availability of renewable energy sources [2,7]. Solar and possibly geothermal energy could be good alternatives to fossil fuels because they are abundantly available, especially in regions that face water shortages [8]. Among several options to connect seawater desalination systems to solar power plants, the combination of a thermal desalination system such as multi effect distillation (MED) and a solar trough field as the heat source is one of the most promising [1]. Solar desalination systems are classified into two categories based on solar energy collection technologies, direct and indirect. In direct collection systems, solar energy is directly used to produce distillate in the solar collector, whereas in indirect systems, one subsystem is employed to collect the energy and the other to desalinate water [1]. Fig. 1 shows the classification of solar desalination systems [9].

Since renewable energy-powered desalination systems are energy-intensive, energy analyses are used to assess and improve their performance. In addition, exergy analysis is used because energy analysis provides no information on how, where, and how much the system performance is degraded [10]. Exergy analysis usually aims to determine the maximum performance of the system and to identify the equipment in which exergy loss occurs, and to indicate potential thermodynamic improvements [11,12]. Thermo-economics combines the principles of thermodynamics and economics to provide useful information on cost-effective energy conversion systems that conventional energy and economic modeling do not usually yield. The thermoeconomic approach has been used to distribute the cost of the entire desalination process onto internal process streams based on exergy, not energy. The monetary costs

[†]To whom correspondence should be addressed.
E-mail: ckyoo@khu.ac.kr
[‡]The first, second, and third authors have identical collaboration in this review paper.

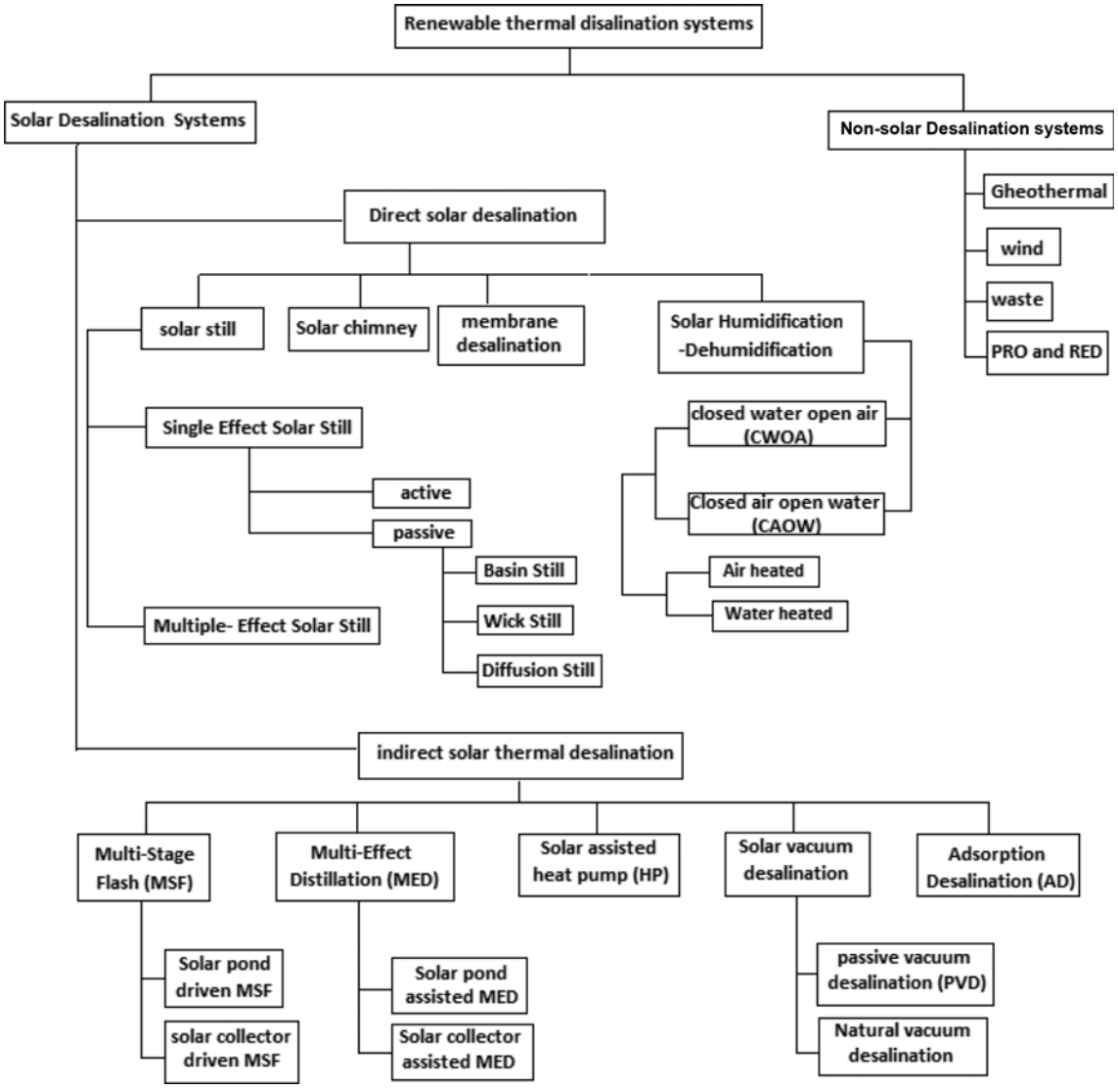

Fig. 1. Classification of solar desalination systems [9,13,46,222,223].

of the process streams, specifically the cost of freshwater, in thermoeconomic analyses are calculated by stream-cost equations that are arranged in a matrix [13].

We present here a comprehensive survey and review of renewable energy-powered thermal desalination systems in thermodynamic, economic, and environmental contexts. We compare REPD technologies based on the direction of energy collection and freshwater production costs. Thermodynamic models of several important processes such as solar basin stills, humidification-dehumidification, and solar chimney processes are presented for determining the energy and exergy efficiency of desalination systems.

PROCESS MODEL AND DESCRIPTION

Renewable thermal desalination technologies are divided into two main categories: solar and non-solar. Solar desalination can either be direct, using solar energy to produce distillate directly in the solar collector, or indirect, combining conventional desalination techniques, such as multistage flash desalination (MSF), vapor compression (VC), reverse osmosis (RO), membrane distillation (MD) and electro dialysis, with solar collectors for heat generation [14]. In indirect systems, solar energy is used either to generate the heat required for desalination and/or to generate electricity that is used to provide the required electric power for conventional desalination plants such as ME, MSF or RO systems [15].

1. Solar Desalination

1-1. Direct Solar Desalination

Direct solar desalination requires large land areas and has a relatively low productivity compared to indirect technologies. However, it is competitive with indirect desalination in small-scale production contexts due to its relatively low cost and simplicity [14]. Direct solar desalination systems can be categorized as solar stills, solar humidification-dehumidification, and solar chimneys as shown in Fig. 1.

1-1-1. Solar Stills

The direct solar desalination method is suited for small produc-

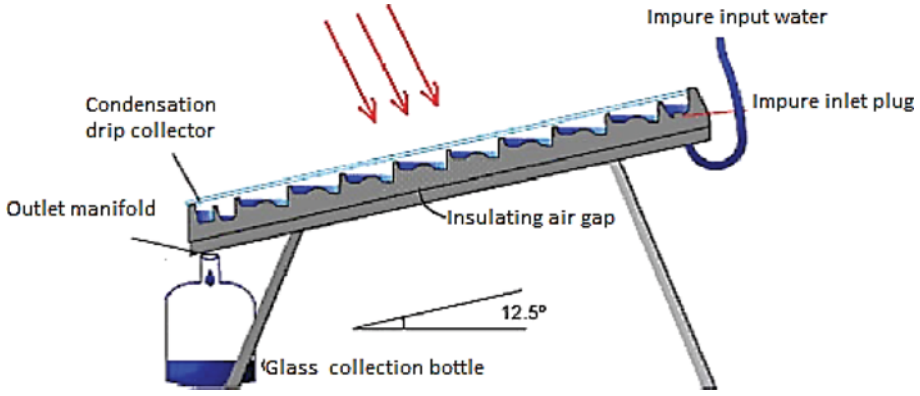

Fig. 2. Simple solar still [224].

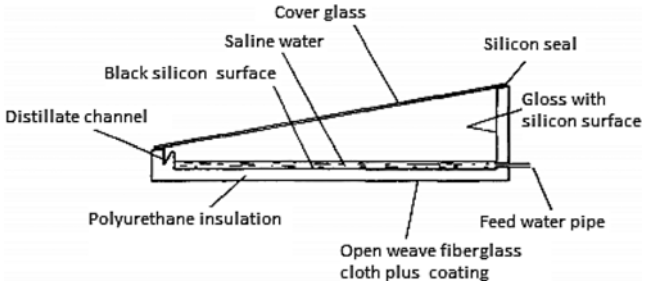

Fig. 3. Cross section of a single effect solar still [225].

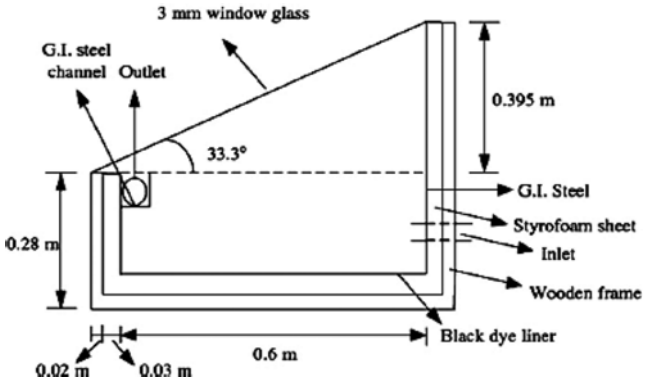

Fig. 4. A schematic of basin solar desalination [177].

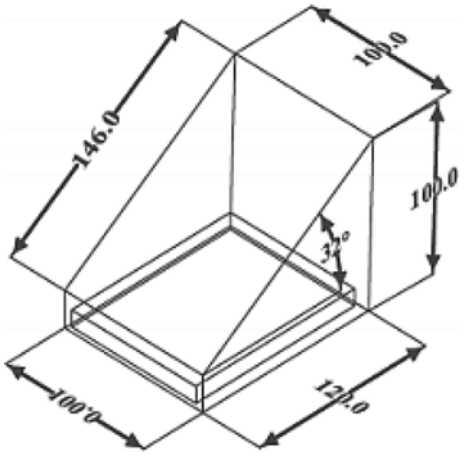

Fig. 5. A schematic of a single slope basin still [18].

tion systems, such as solar stills (including single effect solar stills, multi effect solar stills, basin stills, wick stills and diffusion stills) in regions where the freshwater demand is less than 200 m^3/day [16, 17]. Fig. 2 shows a simple basin type solar still, the oldest such method, improvements in the design of which have been made to increase efficiency [18].

1-1-1-1. Single Effect Solar Still

The single effect solar still (SESS) shown in Fig. 3 is a simple device to convert saline water into potable water. The process is the same as that of natural rainfall generation. The SESS heats water using solar energy, which causes water to evaporate and then condense. The resulting product is high quality drinkable water without salts, inorganics, or microbes. A solar still is made up of a brackish basin with a glass or plastic cover, with glass used for long-term and plastic for short-term applications [14]. The desalination yield is between 4 and 5 l/m^2/day practically [19]. As 5 L/day is the typical potable water requirement per person, 1-1.3 m^2 of solar still is needed per person. SESS desalination has low thermal efficiency, which can be improved by using different passive and active methods.

1-1-1-2. Basin Still

Basin solar stills (BSS) of the type shown in Fig. 4 include a thin layer of water, a transparent glass cover over the water basin, and a channel for collecting the distillate water from solar still. Radiation is transmitted through the glass, heats the saline water in the basin or solar still, and is absorbed by the bottom of the solar still [20]. BSS are categorized as (1) single slope basin stills (SSBSS) and double slope basin stills (DSBSS), (2) stills with cover cooling, and (3) stills with treated cover surfaces [21].

SBSS are fabricated easily using locally available materials like wood and aluminum [20]. In cold climates SSBSS (Fig. 5) works better than double slope stills, but the opposite is true in warm climates or during summer [22]. Water evaporation rates may be increased by increasing the temperature difference between the heat sink and source [23]. This may be achieved for solar stills with cover cooling by flowing cooling water between double cover glasses [14] as shown in Fig. 6. Moreover, if a passive condenser is added to an SSBS as shown in Fig. 7, efficiency can be improved

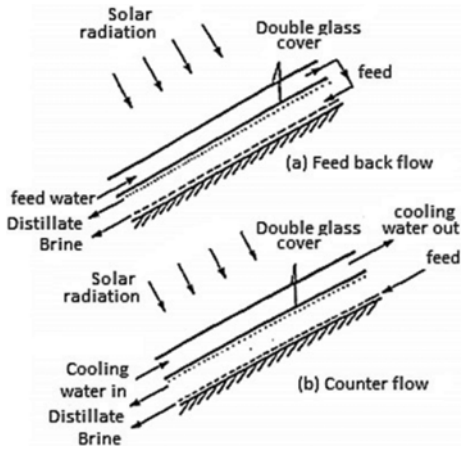

Fig. 6. A solar still with cover cooling by (a) feedback and (b) counter flow [18].

by 45% [9]. The yield can also be increased by using black dye in the seawater. A comparison between single slope and double slope basin stills is shown in Fig. 8.

Setoodeh et al. [24] developed a model to calculate yield for basin type solar stills by applying two-phase three-dimensional model using CFD. They found that estimates of productivity and

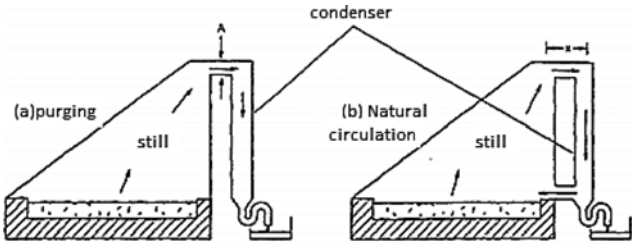

Fig. 7. Single-sloped still with passive condenser [221].

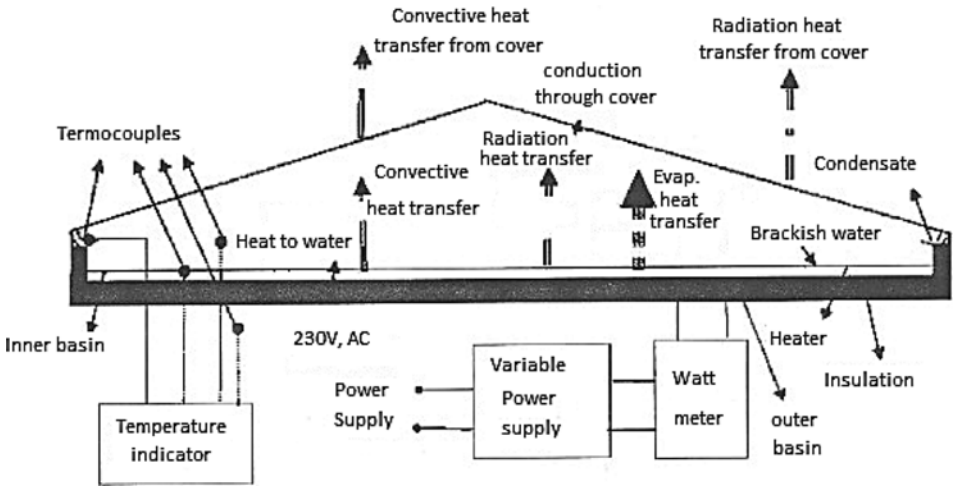

Fig. 8. Double sloped still [19].

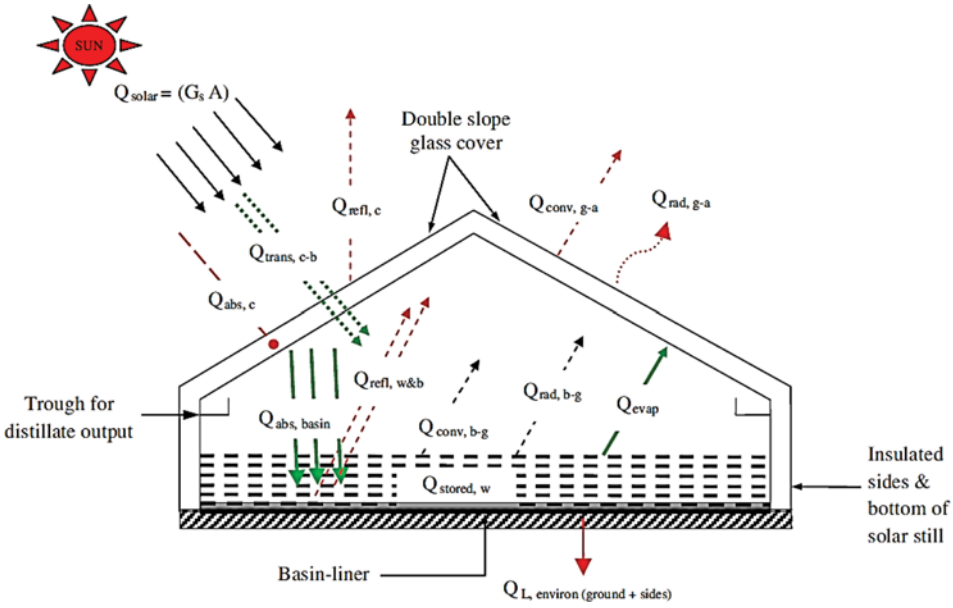

Fig. 9. The major energy transfer mechanism in a single effect double slope basin type conventional solar still [23].

temperature of fresh water obtained using the model have good agreement with experimental data, and therefore concluded that CFD is a powerful tool for solar still modeling.

The major energy transfer mechanism in a single effect double slope basin type conventional solar still is shown in Fig. 9. The corresponding heat transfer model equations developed by Ranjan and Kaushik [25] under steady state conditions are summarized in Table 1.

1-1-1-3. Wick Stills

Wick is a porous, radiation-absorbing padding in which water flows slowly. Sodha et al. [26] described two advantages of wick stills over basin stills: first, the wick can be tilted so that reflection can be reduced and the effective area increased, and second, less feed water is in the still at any time so the water is heated more quickly and to a higher temperature. Simple wick stills as shown in Fig. 10 are more efficient than basin stills, and the costs of cer-

Table 1. Heat transfer model of solar basin

Description	Equation	No	Ref.
Energy analysis	$\sum E_i+\sum_{j=1}^{n} Q_j=\sum E_o+W_{net}$	(1)	[195]
Exergy analysis	$\sum E_{xi}+\sum E_x^Q=\sum E_{xo}+\sum E_{xw}+IR \text{ or } E_{xd}$	(2)	[195]
Exergy transfer	$\sum E_x^Q=W_{max}=Q\left(1-\frac{T_0}{T}\right)$	(3)	[195]
Destroyed exergy	$IR \text{ or } E_{xd}=W_{max}-W_{actual}=W_{lost}$	(4)	[195]
Solar exergy	$E_{xsun}=G_sA\left[1+\frac{1}{3}\left(\frac{T_0}{T}\right)^4-\frac{4}{3}\left(\frac{T_0}{T_s}\right)\right]$	(5)	[23]
Exergy efficiency of the solar distillation system	$\eta_{ex}=\frac{\text{exergy output of a solar still}}{G_sA\left[1+\frac{1}{3}\left(\frac{T_0}{T}\right)^4-\frac{4}{3}\left(\frac{T_0}{T_s}\right)\right]}$	(6)	[196]
Energy balance equation on the saline water body in the basin	$(\tau_c\alpha_b)G_s=q_e+q_{r,\,b-g}+q_{c,\,b-g}+q_L+C_b\frac{dT_b}{dt}$	(7)	[23]
Solar energy absorbed by glass cover	$q_e+q_{r,\,b-g}+q_{c,\,b-g}+G_s\alpha_g=q_{c,\,g-a}+q_{r,\,g-a}+C_a\frac{dT_g}{dt}$	(8)	[23]
Radiation exchange between basin and glass cover	$q_{r,\,b-g}=0.9\sigma(T_b^4-T_g^4)$	(9)	[197]
Convection energy transfer from basin to the glass cover	$q_{c,\,b-g}=h_{c,\,b-g}(T_b-T_g)$	(10)	[197]
Convective heat transfer coefficient between the water surface and the glass cover	$h_{c,\,b-g}=0.884\left[(T_b-T_g)+\left\{\frac{(P_{wb}-P_{wg})}{268.9\times10^3-P_{wb}}\right\}T_b\right]^{1/3}$	(11)	[197]
Evaporative heat transfer, qe from water surface to glass cover	$q_e=16.273\times10^{-3}h_{c,\,b-g}(P_{wb}-P_{wg})$	(12)	[20]
Exergy destruction (irreversibility) in the collector or basin liner	$E_{x_{d,\,b}}=\varepsilon_{col}E_{x_{sun}}-(E_{x_w}+E_{x_{insul}})$	(13)	[23]
Exergy balances on the saline water according	$E_{x_{d,\,w}}=E_{x_w}-E_{x_{t,\,w-g}}$ and $E_{x_{d,\,g}}=E_{x_{t,\,w-g}}-E_{x_{t,\,g-a}}$	(14)	[23]
Exergy efficiency of collector basin liner	$\eta_{ex,\,b}=\frac{E_{x_w}}{E_{x_{sun}}}$	(15)	[23]
Exergy efficiency of evaporation from saline water	$\eta_{ex,\,evap}=\frac{E_{x_{e,\,w-g}}}{E_{x_w}}$	(16)	[23]

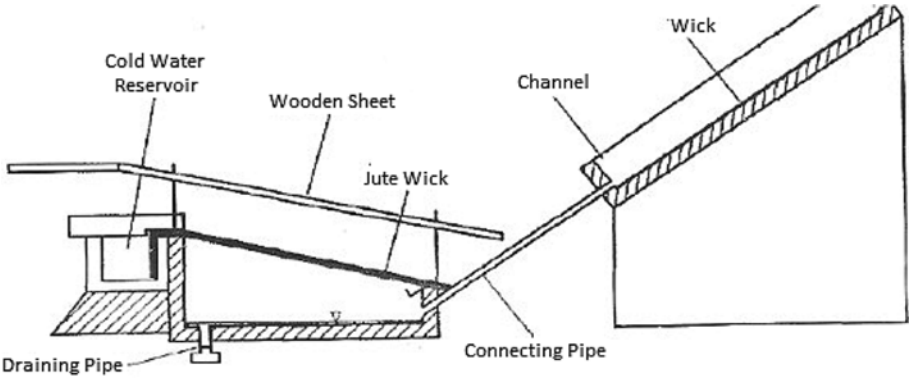

Fig. 10. Wick basin type solar still [52].

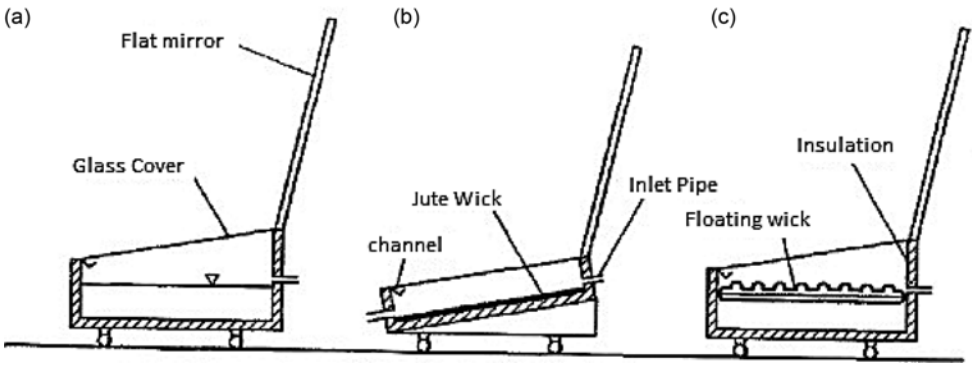

Fig. 11. Floating wick type solar still [25].

tain designs are less than those for basin stills of the same output.

Wick stills are reported to be efficient and economic systems for producing fresh water [14]. The water production of floating wick type solar stills is higher than that of other types of solar stills [27]. Absorbers such as jute wicks and char coal wicks, cotton cloth, and floating perforated black aluminum plates in the basin can affect the yield of solar stills [14].

For a floating wick type solar still as shown in Fig. 11 the water layer thickness is calculated as follows [27]:

$$\Delta Y \le \sqrt{\frac{kw}{\frac{\rho_w c_{pw}}{\Delta\tau} - U_2 A_s}} \quad (1)$$

where kw is thermal conductivity of water (w/m K), ρ_w is density of water (kg/m^3), c_{pw} is specific heat capacity of water (J/kg K), $\Delta\tau$ is selected time interval (2 min), U_2 is overall heat transfer coefficient between the bottom wall and surrounding (W/m^2 °C), and A_s is area of the still (m).

The rate of condensation for each time interval is calculated for the mean values of meteorological data such as solar intensity, wind speed, and ambient temperature, as follows [27]:

$$m_{int}(j) = \frac{h_{cond}(T_w - T_{gi})}{\lambda}\Delta\tau \quad (2)$$

where, T_w and T_g are water and glass temperatures (°C), and the hourly productivity, m_i, i=1, 2, R=3600/$\Delta\tau$. If W is the number of operating hours per day, then daily productivity (Pd) is obtained as [27]

$$P_d = \sum_{i=1}^{w} m_i \quad (3)$$

1-1-1-4. Diffusion Stills

Diffusion stills are combinations of a heat tank with a solar collector and distillate unit. One design of diffusion stills is the four-effect still. Per 1 m^2 active cross-section of the apparatus, 4 m^2 surface of evaporator and condenser, and energy input of 2.0 kWm^{-2}, the theoretical distillate output is 8.7 kg m^{-2} h^{-1} [28].

1-1-1-5. Multiple-effect Solar Stills

In multiple effect solar still (MESS) systems the condensation latent heat is reused, making them more efficient than (SESS) [29]. The re-utilization of latent heat in two or more stages is known as a multi effect distillation system. Their higher efficiency leads to higher capital and operating costs [29]. The additional production resulting from multi-effect stills justifies the additional cost [21]. The production rate of a unit investigated by [29] reached 25 L/m^2/day, for a value of 4.8 kW h/m^2/day of solar radiation. The classification of MESS is the same as of SESS. The main innovations of

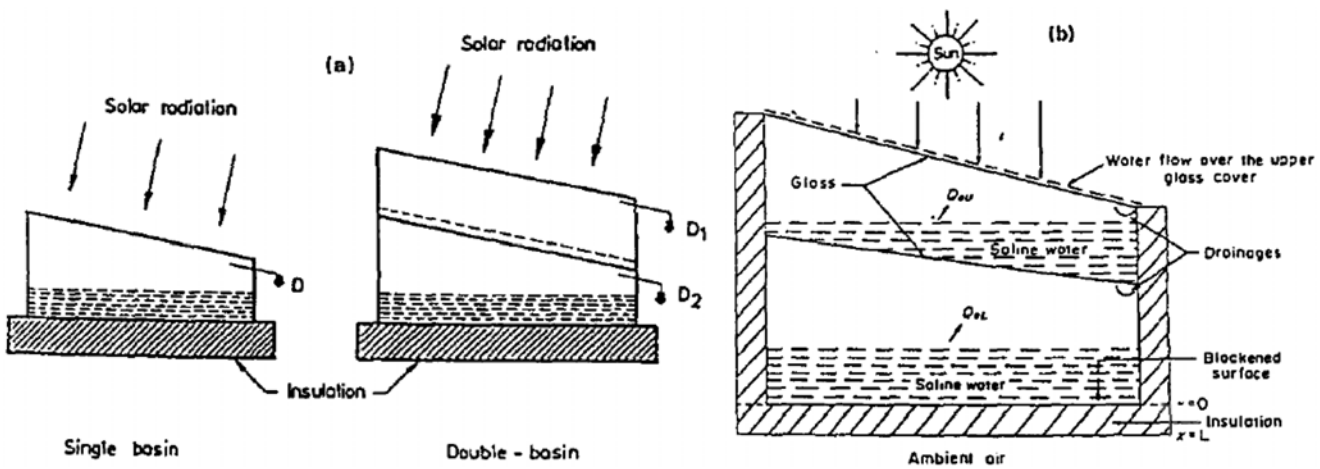

Fig. 12. Double-basin solar stills. (a) Schematic of single and double-basin stills. (b) Stationary double-basin still with flowing water over upper basin [19].

multi-stage stills are double effect basin stills, (DEBS), multi-effect multi-wick stills (MEWS), and multi-effect diffusion stills [21].

In DEBS, water from the second basin can either flow over the glass cover (Fig. 12(a)) or remain stationary (Fig. 12(b)) [21]. Sodha et al. [30] showed that double-basin type stills produced about 56% higher yield than single effect stills. In multi-effect multi-wick type solar stills (Fig. 13) the availability of latent vaporization heat is maximized and equalized for least water depths in each effect,

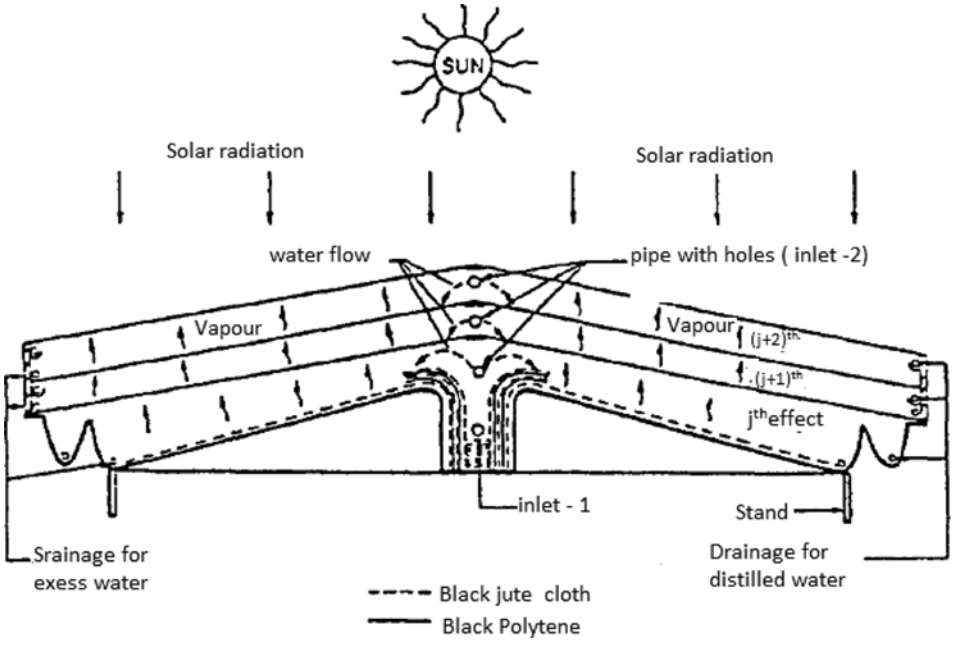

Fig. 13. A schematic of a multi-effect multi-wick solar still [24].

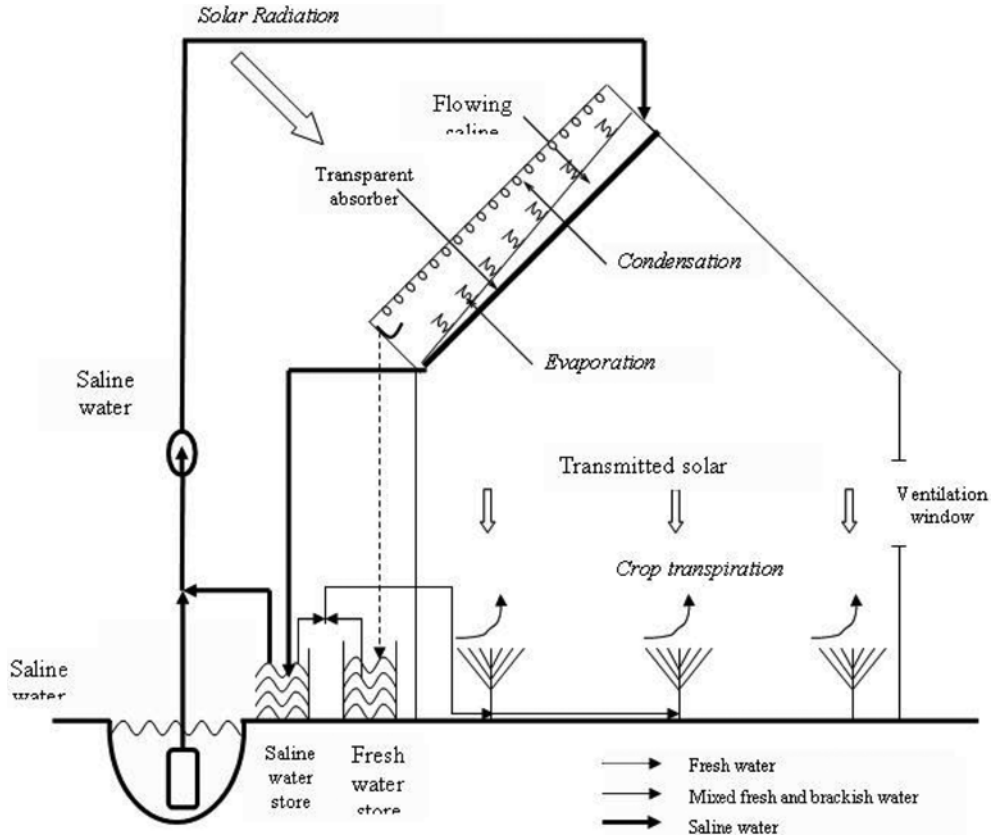

Fig. 14. System principles for water desalination integrated in a greenhouse roof [44].

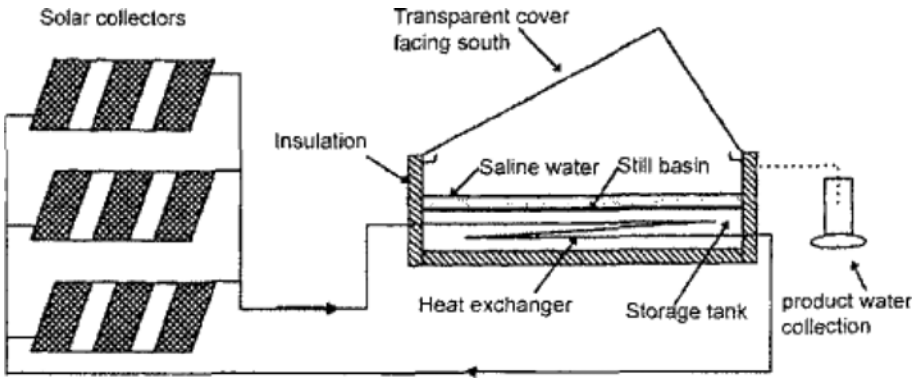

Fig. 15. Diagram of a solar still and water heating system (PV/T) active solar still [32].

including the lower basin [26].

1-1-1-6. Solar Still Greenhouse Combination

Solar still greenhouse combinations (Fig. 14) are interesting designs for locations where saline or brackish water is available [22]. This type integrates a solar still with a greenhouse environment for cultivating crops and can produce sufficient water for its own use [31].

Chaibi and Jilar [32] developed an integrated solar system greenhouse based on the Bettaque system. In their system, solar radiation is absorbed by a layer of water flowing on glass that is covered by a top glass, so that roof light transmission is reduced. Fresh water evaporates, condenses on the top glass, and is collected at the roof eaves.

1-1-1-7. Externally Heated (Active) Solar Stills

To increase the temperature of saline water, external heating can be accomplished using a solar heater or a solar concentrator and waste heat recovery system [14]. If phase change material is added and the latent heat is reused, the yield will also increase [33].

Coupling a solar still with a solar collector and storage tank will increase yield. The input- output method can be used to estimate yield with an accuracy of 3%. Hybrid behavior can be applied during the design or usage of such systems. Fig. 15 shows a schematic hybrid diagram of a solar still and water heating system [34].

1-1-2. Water Desalination with Humidification-dehumidification

Direct contact of saline water with the collector may corrode the still, negatively impacting still performance and efficiency [35]. To solve this problem, humidification-dehumidification desalination (HDH) systems have been developed, in which the working fluid is air. Air can be humidified with notable amounts of vapor; 1 kg of dry air can carry 0.5 kg of vapor and about 670 kcal energy, while increasing the temperature from 30 to 80 °C. Fresh water is produced during the air dehumidification process. This provides a means for low pressure, low temperature desalination and is very

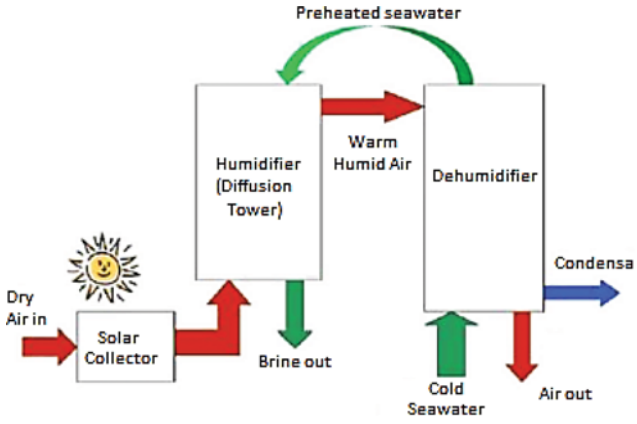

Fig. 16. A simple humidification-dehumidification process [13].

cost competitive [36] with many other methods, but not with reverse osmosis and the multistage flash evaporation [37]. For multi-effect humidification the yield is about 6,000 L/month [38]. Müller-Holst et al. [39] reported 500 L/day yield for a solar MEH-desalination system with a 38 m^3 collector area. The HDH system has other merits, including much simpler brine pre-treatment, disposal requirements, simplified operation and maintenance [14]. Fig. 16 shows a schematic of the humidification-dehumidification process.

HDH systems are classified into three broad categories based on the form of energy used, the cycle configuration, and the type of heating used [14], as summarized in Table 2. The specific water production is between 4 and 12 kg/m^2 day and the GOR varies between 1.2 and 4.5. These GOR values translate into energy consumption rates ranging from 140 to 550 kWh/m^3, which are higher than those of conventional technologies such as MSF or RO. RO plants, which are the most energy efficient, consume 4 to 10 kWh/m^3 [14].

Table 2. Classification of HDH systems under three categories [13]

Form of energy used	Cycle configuration	Type of heating used
• Solar • Thermal • Geothermal	• Closed-water open-air (CWOA); air is heated, humidified and partially dehumidified and let out in, the process is shown in Fig.17(a) • Closed-air open-water (CAOW); air is circulated in a closed loop between the humidifier and the dehumidifier the process of CAOW is shown in Fig. 17(b).	• Water heating system • Air heating system

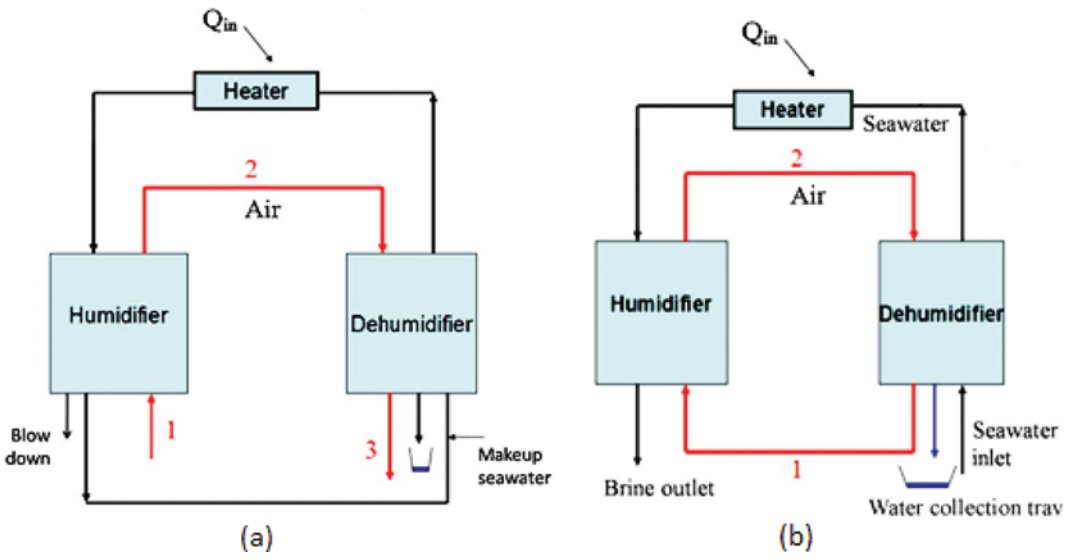

Fig. 17. (a) A typical water-heated CWOA HDH process. (b) A typical water-heated CAOW HDH process [13].

Humidifier efficiency can be obtained using the h-x diagram shown in Fig. 18 as follows [40]:

$$\eta_w = 100\{(x_2 - x_1)/(x_3 - x_1)\} \quad (4)$$

where x_1 and x_2 are inlet humidity and maximum achievable saturation humidity.

The water enthalpy reduction will be identical to the enthalpy increase of air

$$\dot{m}_l \cdot \Delta h_L = cp_w \cdot \dot{m}_w \cdot (t_{wi} - t_{wA}) \rightarrow \Delta h_L = \frac{\dot{m}_w}{\dot{m}_l} \cdot cp_w \cdot \dot{m}_w \cdot (t_{wi} - t_{wA}) \quad (21)$$

where $\dot{m}_l$ is air flow rate, kg/h; $\dot{m}_w$ is flow rate of injected water, kg/h; t_{wi} is water inlet temperature, °C; t_{wA} is water outlet temperature, °C; cp_w is specific heat of water, kJ/kg and Δh_L is enthalpy change of air flow, kJ/kg [40].

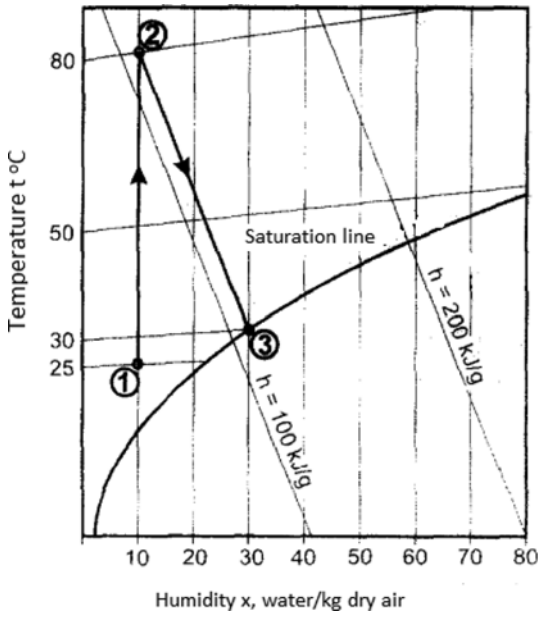

Fig. 18. An h-x diagram to define humidification efficiency, 1 to 2 heating processes, 2 to 3 humidifying processes.

1-1-2-1. Gained-output-ratio (GOR)

The gained-output-ratio (GOR) is the ratio of the latent heat of evaporation of the distillate produced to the total heat input absorbed by the solar collector [14]. Shaobo et al. [41] used Pinch technology in both humidification and dehumidification processes to determine the maximum temperatures of saturated air, rejected water, and water leaving the heat exchanger. Considering the diagram of the HDD process shown in Fig. 18, and the thermodynamic data of the thermal system, the relationship of T and H is:

For feed sea and spraying seawater:

$$H_{water} = 4.1868 \dot{m}_{water} T = 4.1868 \text{RatioT} \quad (5)$$

and for the saturated air:

$$H_{air} = \exp(2.39329 + 0.10648T - 0.00135T^2 + 0.000010058T^3) \quad (6)$$

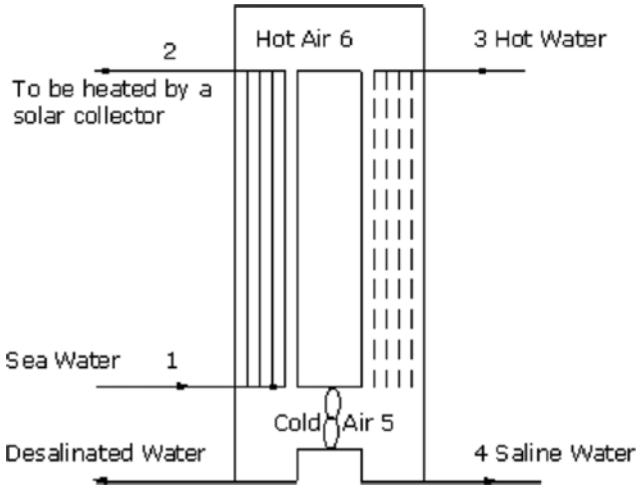

Fig. 19. Sketch of a humidification-dehumidification desalination process [39].

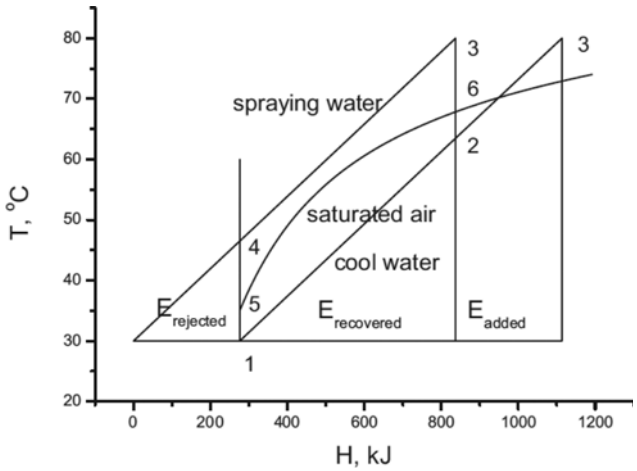

Fig. 20. The hot and cold curves of humidification and dehumidification processes when the ratio=4 [39].

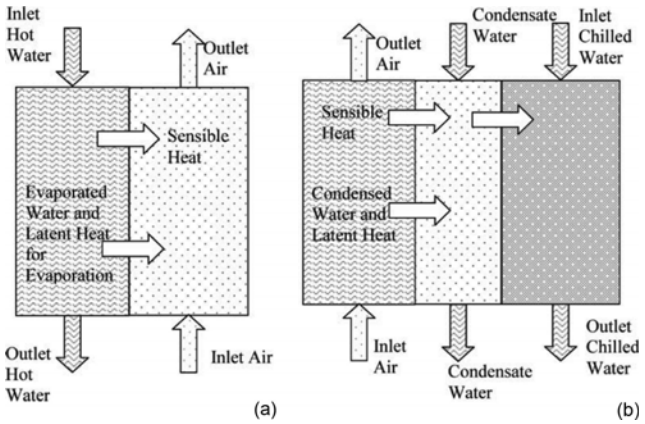

Fig. 21. A schematic of heat and mass transfer taking place in (a) humidifier and (b) condenser [42].

Table 3. Mathematic model for the humidification dehumidification [42]

Description	Mathematical model	No.
Condenser heat transfer area	$m_c Cp_c(T_{co}-T_{ci})=U_c A_c LMTD_c$	(26)[a]
	$LMTD_c=\frac{(T_{a2}-T_{co})-(T_{a3}-T_{ci})}{\ln\left(\frac{T_{a2}-T_{ci}}{T_{a3}-T_{ci}}\right)}$	(27)[b]
Humidifier energy balance	$LCp_w(T_{wi}-T_{wo})=G(H_{a2}-H_{a1})+Q_h$	(28)
Condenser energy balance	$m_c Cp_c(T_{co}-T_{ci})=G(H_{a2}-H_{a1})-Q_c$	(29)
Overall mass transfer coefficient	$(G/L)(H_{a1}-H_{a2})=(kaV/L)\frac{(H_{wi}-H_{a2})-(H_{wo}-H_{a1})}{\ln\frac{(H_{wi}-H_{a2})}{(H_{wo}-H_{a1})}}$	(30)
Production flow rate	$m_d=G(W_{a3}-W_{a2})$	(31)
Model correlations		
Humid air density	$\rho_a=\frac{(1+W)M_a P_a}{R(1+1.6078W)(273.15+T_a)}$	(32)
Absolute humidity of air	$W=0.62198\frac{P_d}{(P_a-P_d)}$	(33)
Air enthalpy	$H_a=(Cp_a+1.88)T_d+W_a\lambda$	(34)
Water specific heat at constant pressure	$Cp=\left(\begin{matrix}4206.811262T+1.2026\times10^{-2}T^2\\+6.8777\times10^{-7}T^3\end{matrix}\right)\times10^{-3}$	(35)
Latent heat for water evaporation	$\lambda=\left(\begin{matrix}2501.897149=2.407064037T+\\1.92217\times10^{-3}T^2-1.5863\times10^{-5}T^3\end{matrix}\right)$	(36)
Water vapor pressure at the dry bulb temperature	$P_d=\phi P_s$	(37)
Water vapor saturation pressure at the dry bulb temperature	$\ln(P_s/P_c)=\left(\frac{T_c}{T_d+273.15}-1\right)\times\sum_{i=1}^{8}f_i(0.01(T_a+273.15-338.15))^{i-1}$	(38)

[a] m_c is the cooling water flow rate in the condenser (kg/s), C_{pc} is the specific heat at constant pressure of the cooling water (kJ/kgK), T_{co} and T_{ci} are outlet and inlet cooling water temperatures (°C), U_c is the overall heat transfer coefficient of the condenser (kW/m^2 °C), A_c is the condenser heat transfer area (m^2)

[b] $LMTD_c$ is the condenser logarithmic mean temperature difference, T_{a3} and T_{a2} are the outlet and inlet air stream temperatures to the condenser (°C)

Determining the minimum approach temperature for both processes, and obtaining hot and cold curves on a single chart, the least energies that should be added, recovered, and rejected are determined as follows:

$$E_{rec}=H_6-H_5-E_{added} \quad (7)$$

Points from 1 to 6 in an HDH process are shown in Fig. 19, and a T-H diagram of these points is shown in Fig. 20.

The thermal energy recovery rate, k, can be obtained as follows [41]

$$k=\frac{E_{rec}}{H_6-H_5} \quad (8)$$

When temperature differences decrease at the pinch point, re-

Table 4. Mathematical model of HDh developed by Zhani [43]

	Equations	No.
Water solar collector	$\frac{dT_w}{dx}=\frac{U_w l}{m_w C_w}\left(\frac{\tau\alpha l}{U_w}+T_{amb}-T_w\right)$	(39)[a]
Evaporation tower: water phase	$\frac{dT_1}{dz}=\frac{h_1 a(T_l-T_g)}{LC_1}$	(40)[b]
Evaporation tower: air phase	$\frac{dT_g}{dz}=\frac{h_g a(T_i-T_g)}{GC_g}$	(41)
Evaporation tower: air-water interface: thermal	$W_i=W_g+\frac{h_l a(T_l-T_i)+h_g a(T_i-T_g)}{\lambda_o k_g a}$	(42)
Evaporation tower: air-water interface: mass	$\frac{dW_g}{dz}=\frac{k_g a(W_i-W_g)}{G}$	(43)
Evaporation tower: mass exchange coefficient	$k_g=\frac{2.09G^{0.11515}L^{0.45}}{a}$	(44)[c]
Evaporation tower: heat exchange coefficient	$h_l=\frac{5900G^{0.5894}L^{0.169}}{a}$	(45)
Condensation tower: water phase	$\frac{dT_e}{dz}=\frac{UA(T_{ic}-T_e)}{D_e C_e}$	(46)
Condensation tower: air phase	$\frac{dT_G}{dz}=A\frac{(h_G(T_G-T_{ic})+\lambda_o k_G(W_G-W_{ic}))}{GC_G}$	(47)
Condensation tower: air-condensate interface: heat	$W_{ic}=W_G+\frac{h_G(T_G-T_{ic})+U(T_e-T_{ic})}{\lambda_o k_G}$	(48)
Condensation tower: air-condensate interface: mass	$\frac{dW_G}{dz}=\frac{k_G A(W_G-W_{ic})}{G}$	(49)
Condensation tower: water balance equation	$dm_c=GdW_G$	(50)
Condensation tower: flow rate of the condensed water	$dm_c=k_G A(W_{ic}-W_G)dz$	(51)
	$U=\frac{1}{\left(\frac{1}{h_c}\right)+\left(\frac{e}{\lambda_P}\right)+\left(\frac{1}{h_e}\right)}$	(52)[d]
Overall heat transfer coefficient	$h_e=0.023\frac{\lambda_e}{D_{h2}}Re^{0.8}Pr^{0.33}$	(53)
	$h_c=\sqrt[4]{\frac{\rho_c^2 g\lambda_o\lambda_c^3}{4\mu_c z(T_{ic}-T_p)}}$	(54)
Output ratio	$GOR=\frac{m_c\lambda_o}{LC_i(T_{l2}-T_{l1})}$	(55)[e]
Thermal efficiency	$\eta=\frac{m_w C_w(T_{wo}-T_{wi})}{IS}$	(56)[f]

[a]There is no mass or concentration change collector that can be modeled solely from thermal energy balances

[b]The model is developed using thermal and mass balance for water and air face and also air-water interface

[c]G=air flow rate, L=water flow rate

[d]From the air-condensate interface to the cooling water inside the condenser

[e]m_c is the condensation flow rate, L is the water mass flowrate in the evaporation tower, and λ_o is the latent heat of vaporization

[f]m_w is the water mass flow rate, C_w is the water heat capacity, T_{wo} is the water outlet temperature, T_{wi} is the water inlet temperature, I is the solar irradiation intensity and S is the collector area

covery of thermal energy increases [41,42]. The two-stage solar multi-effect HDD has a higher energy recover rate than the one-stage type with 1 °C as the minimum temperature difference at the pinches, with an energy recovery rate of 0.836 [42], while the recovery rate of the one-stage type is 0.75 [41]. If the energy recovery rate reaches 0.9, the GOR increases significantly [42]. Hallaj et al. [43] showed that the HD process powered by waste heat is superior to other conventional processes based on waste heat, including GOR, and that the capital cost for the higher production capacity of HDH is lower [43].

The mathematical model for the humidification dehumidification system shown in Fig. 21 is summarized in Table 3. The production rate is strongly affected by hot and cooling water temperatures. High hot water temperature, low cooling water temperature, high air flow rate, and low hot water flow rate result in the highest production rates, heat transfer, and mass transfer coefficients [44].

Khalifa [45] developed a mathematical model in steady state regimes based on heat and mass transfer in the water solar collector, evaporation tower, and condensation tower of desalination systems to numerically simulate HDH. This model is summarized in Table 4.

1-1-3. Solar Chimney Desalination

1-1-3-1. Solo Solar Chimney (SSCh)

Solar chimneys convert solar thermal energy into kinetic energy, which can be converted into electrical energy using a turbo-generator. The main components of a solar chimney are large diameter solar collectors, turbines, generators, and long chimneys. A solar chimney is a combination of three established technologies: the greenhouse, the chimney, and the wind turbine. The chimney, which is a long tubular structure, is placed in the center of the circular greenhouse, while the wind turbine is mounted inside the chimney [46]. The kinetic energy of the moving air causes rotation of the turbine mounted below the chimney to produce power [47]. Compared to conventional solar chimney power plants, sloped solar chimney power plants are more efficient and provide smoother power output [48]. The electrical power from the solar chimney to the grid is calculated as follows [47]:

$$P_{out} = \frac{2}{3}\eta_t \eta_{coll} \frac{g}{C_p T_a} H_{ch} A_{coll} q \quad (9)$$

where η_{coll} is the efficiency of the collector, η_{ch} is the efficiency of the chimney, and η_t is the efficiency of the wind turbine generator.

1-1-3-2. Solar Chimney Desalination (SChD)

Lu et al. [48] studied the integration of desalination systems with solar chimney power plants as shown in Fig. 22. The integrated system consists of five major components: chimney, collector, turbine, energy storage layer, and basin solar still. Below the energy collector, the basin still and rock energy storage layer serve as an absorber bed. They found that solar stills are cheap and have low maintenance costs, but the small amount of water produced was unacceptable [49]. The reasons for this poor production include [50]:

- The latent heat of condensation of water vapor released at the inner surface of the still cover is not reutilized and is wasted to the ambient air;
- The use of natural convective heat transfer mode in solar stills greatly limits the improvement of thermal performance of stills;

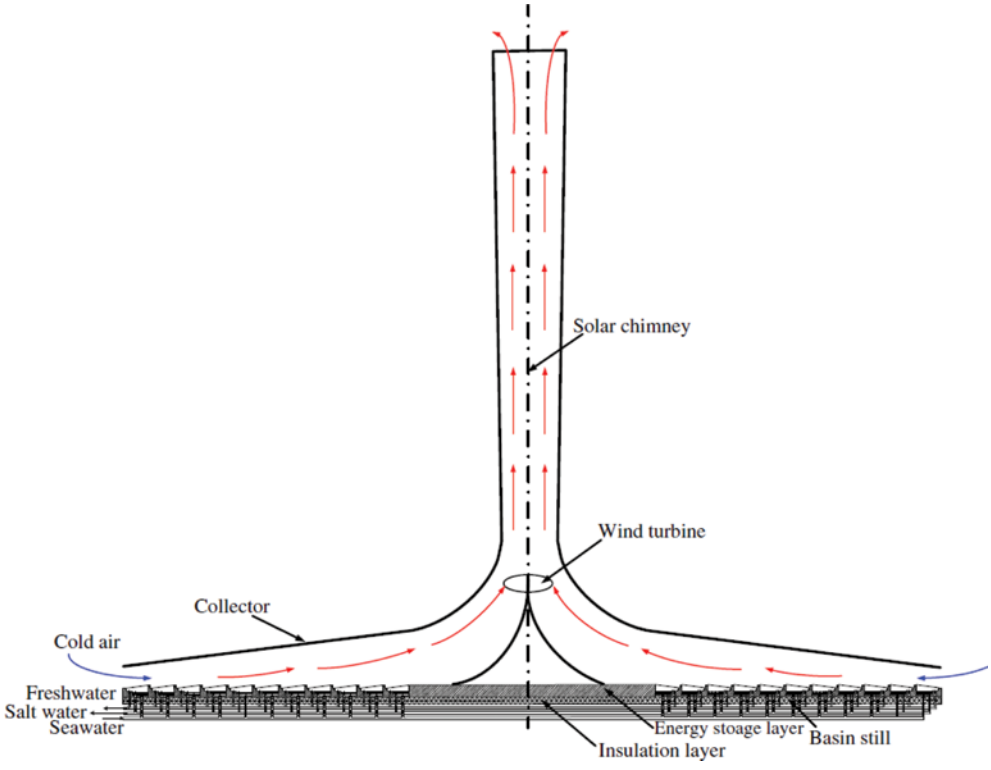

Fig. 22. Schematic diagram of solar chimney desalination [49].

Table 5. Performance analysis of solo solar chimney power system [49]

Description	Performance analysis	No
SSCS: airflow	$q_{cp,m}+q_{cg,m}=-\frac{c_{p,m}M_m}{2\pi r}\frac{\partial T_m}{\partial r}$	(58)
	$q_{cg,m}=h_{cg,m}(T_g-T_m)$	(59)[a]
	$q_{cp,m}=h_{cp,m}(T_p-T_m)$	(60)[b]
SSCS: collector roof	$q_{cm,g}+q_{rp,g}+\alpha_g\cdot I=q_{rg,s}+q_{cg,a}$	(61)[c]
SSCS: black absorber	$\alpha_p\cdot\tau_g\cdot I=q_{cp,m}+q_{kp}+q_{rp,g}$	(62)[d]
SSCS: velocity of hot air flow at chimney inlet	$V_{ch}=\sqrt{2gH_{ch}\frac{T_{ch,in}-T_a}{T_a}}$	(63)
SSCS: power output	$P_e=\frac{1}{3}\eta_t\rho_{ch,in}A_{ch}V_{ch}^3=\frac{1}{3}\eta_t\rho_{ch,in}\left(\frac{1}{4}\pi D_{ch}^2\right)\left(2gH_{ch}\frac{T_{ch,in}-T_a}{T_a}\right)^{3/2}$	(64)
SSCS: daily utilization efficiency of solar energy	$\eta=\frac{P_e}{\frac{1}{4}(\pi)(D_{coll}^2-D_{ch}^2)\cdot I}$	(65)
Integrated system: air flow	$q_{cc,m}+q_{cg,m}=-\frac{c_{p,m}M_m}{2\pi r}\frac{\partial T_m}{\partial r}$	(66)
Integrated system: collector roof	$q_{cm,g}+q_{rc,g}+\alpha_g\cdot I=q_{cg,a}+q_{rg,s}$	(67)
Integrated system: glass cover	$q_{e,w}+q_{cw,c}+q_{rw,c}+\alpha_c\cdot\tau_g\cdot I=q_{cc,m}+q_{rc,g}$	(68)
Integrated system: sea water	$\alpha_w\cdot\tau_c\cdot\tau_g\cdot I+q_{b,w}=q_{e,w}+q_{rw,c}+q_{cw,c}+c_{p,w}M_w\frac{dT_w}{d\tau}$	(69)
Integrated system: pond bottom plate	$\alpha_b(1-\alpha_w)\cdot\tau_c\cdot\tau_g\cdot I=q_{b,w}+q_{b,ins}$	(70)
Integrated system: daily utilization efficiency of solar energy	$\eta=\frac{\frac{1}{4}(\pi)(D_{coll}^2-D_{xu}^2)q_{ew}+P_e}{\frac{1}{4}(\pi)(D_{coll}^2-D_{ch}^2)\cdot I}$	(71)
Integrated system: hourly productivity of fre water	$m_e=\frac{q_{ew}}{h_{fg}}\times 3600$	(72)

[a] $q_{cg,m}$: the convective heat transfer rate between the collector roof and the air inside the collector
[b] $q_{cp,m}$ is the convective heat transfer rate between the surface of absorber and the air inside the collector
[c] $q_{rp,g}$ is the radiation heat transfer rate between the surface of absorber and the collector roof, $q_{rg,s}$ is the radiation heat transfer rate between the collector roof and the sky and $q_{cg,a}$ is the convective heat transfer rate between the collector roof and the environment
[d] q_{kp} is the conduction heat transfer rate from the absorber surface to the energy storage layer

• The heating capacity of the sea water that is evaporated is too high, so the enhancement of operating temperature is limited, and therefore the driving force of evaporation is weakened.

Meteorological parameters such as wind velocity, solar radiation, sky temperature, ambient temperature, relative humidity, salt concentration, sea water thickness, algae formation on the water, and mineral layers on basin liners significantly affect the performance of solar stills [49]. Performance analyses of solo solar chimney power systems (SSCh) and integrated systems are summarized in Table 5 [48]. Energy flows through a control volume of SSCh and SChD are shown in Figs. 23 and 24, respectively.

1-1-3-3. Thermal Efficiency

The thermal efficiency of the desalination unit is given by [51]

$$\eta_d=100\frac{\dot{m}_w)_m L_{w,vap}}{\dot{Q}_{in}+\dot{W}_c} \quad (73)$$

where $\dot{m}_w)_m$ is the water measurement productivity; $L_{w,vap}$ is the latent heat of vaporization of water at brackish water temperature in the evaporator chamber; W_c is the power of the compressor. The yield of the system after correlation with a maximum deviation of 7% is [52]

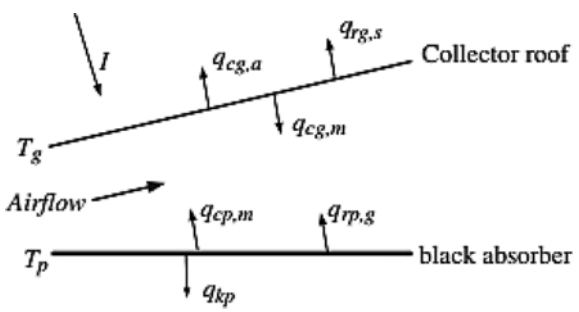

Fig. 23. Energy flow through a control volume of SSCh [49].

$$\dot{m}_w=1.597\times10^{-7}(T_w)^{3.971}\times(0.127+2352\times10^{-7}h)\times(0.87231-0.02473\dot{m}_a) \quad (74)$$

at : $50\le87$ °C; $20\le h\le60$ cm; $4.2\le\dot{m}_a\le14 kg_a/h$

where, $\dot{m}_w)_m$ is the water measurement productivity of the system, $L_{w,vap}$ is the latent heat of vaporization of water at brackish

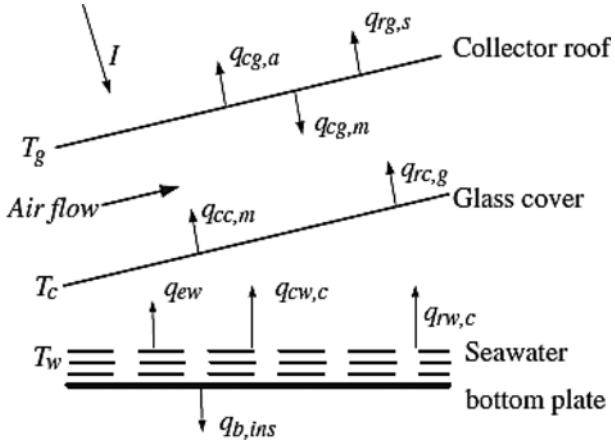

Fig. 24. Energy flow through a control volume of SChD [49].

water temperature in the evaporator chamber and W_c is the power of the compressor.

1-1-4. Membrane Desalination (MD)

Membrane based-desalination processes include reverse osmosis (RO) [53,54], membrane distillation (MD), and electrodialysis (ED). Renewable energy sources can be used to drive membrane desalination systems with lower water production costs compared to the conventional energy sources [55]. Among renewable energies, solar is more appropriate for powering the membrane process. The required energy of RO and ED systems is in the form of electricity, which can be provided by solar photovoltaic, while MD requires mainly thermal energy, which can be provided by solar thermal collectors. PV-powered RO system (PV-RO) system is one of the most promising forms of renewable energy powered membrane process, especially for remote areas. Many PV-RO systems have been installed around the world with energy storage systems to run the system 24 h a day. Among all membrane based-desalination processes, the MD process can be categorized as a hybrid thermal distillation and membrane process. Therefore, in this paper we review the solar powered-MD.

Membrane distillation (MD) as a low cost and energy saving alternative to conventional membrane desalination process is a hybrid of thermal distillation and membrane processes. Since the flux of MD process is lower than the other membrane-separation process such as reverse osmosis, therefore MD is not commercialized yet for large scale freshwater production capacities [56-59]. Fig. 25 shows the principle of membrane distillation in which a hydrophobic microporous membrane separates a warm solution from cooler chamber, which contains either a liquid or a gas. The temperature difference produces a vapor pressure gradient that causes vapor molecules to pass through the membrane and condense on the cooler surface as high purity freshwater. There are several various configuration of MD process based on method of vapor passing through the membrane including, direct contact membrane distillation (DCMD, air gap membrane distillation (AGMD), vacuum membrane distillation (VMD), sweeping gas membrane distillation.

Membrane distillation process can be powered by low-grade and renewable energy sources such as wind, solar, and geothermal. The required heat of the process can be provided by solar energy collectors such as flat plate collectors, vacuum collectors, solar ponds, solar stills, and parabolic troughs [60]. Fig. 26 shows the configuration of a typical solar stand-alone MD desalination system with flat plate collectors.

The coupling of MD systems with solar thermal systems has been studied by several researchers. The first study, done by Hogan et al. [61], described an MD system with capacity of 0.05 m^3/d that used 3 m^2 flat plate solar collectors. They reported that the thermal and electrical energy consumption was 22 kWh/m^3. Thomas [62] installed a solar powered-MD system with a 12 m^2 field of vacuum tube collectors. Banat et al. [63] installed a large MD system with two loops, including desalination loop which operated with seawater and collector loop which operated by a titanium corrosion resistant heat exchanger. Recently, Wang et al. [64] described the performance of a solar-heated hollow fiver vacuum membrane distillation system for freshwater production from underground water. They used an 8 m^2 solar energy collector with a 0.09 m^2 membrane. A solar still-membrane distillation system operated with artificial seawater was investigated by Banat et al. [65]. In their system hot water from the still was circulated into an MD module before returning back to the still. The freshwater was pro-

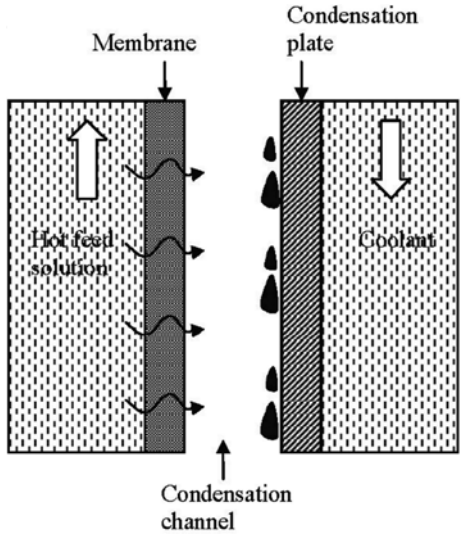

Fig. 25. Principle of the membrane distillation process [45].

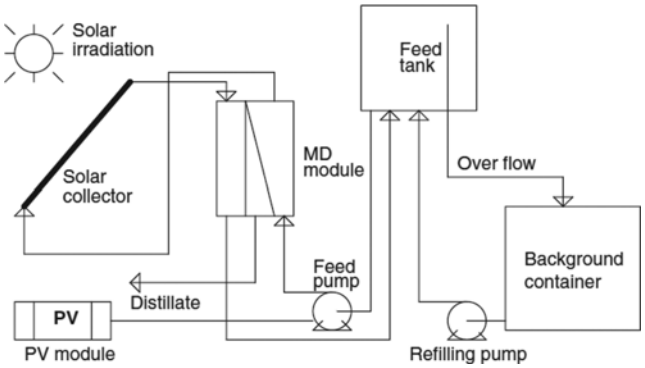

Fig. 26. Solar stand-alone MD desalination system with flat plate collector [70].

duced from both the solar still and MD module. They reported that the flux of membrane distillation module was four-times higher than that from the solar still.

Very few studies have reported the freshwater production costs of the solar powered MD systems. Kullab and Martin [66] estimated 8.9 $/m^3 for a yearly freshwater production of 24,000 m^3. The cost of potable water produced by the stand-alone compact MD unit has been estimated between 15 to 18 $/m^3 by Banat and Jwaied [67]. The MD systems can be integrated with other thermal desalination systems such as MED or MSF to reduce the water production costs.

In membrane desalination systems powered by photovoltaic systems the investment cost is relatively high which leads to increase the water production costs. PV-RO and PV-ED are two commercially applicable systems in this area. Based on published reports by Garcıa-Rodrıguez [68], and Alkhudhiri et al. [58] the freshwater production cost by seawater reverse osmosis is in the range of 7.95 to 29 $/m^3 for units with capacity of 120 to 12 m^3/d. Thomson et al. [69] estimated that the unit freshwater production cost of seawater RO with capacity of less than 100 m^3/d is from 11.7 to 15.6 $/m^3, while the unit freshwater production cost of brackish RO system is from 6.5 to 9.1 $/m^3. Few pilot plants of PV-ED systems with capacities of less than 100 m^3/d have been implemented around the world. The freshwater production cost of these systems is from 5.8 to 16 $/m^3 [70].

The main characteristics of direct solar desalination technologies are summarized in Table 6.

1-1-5. Comparison between Thermal Desalination and Membrane-based Reverse Osmosis

RO as the pioneer membrane-based technology has been competing with thermal desalination technologies in the last decades. Although both thermal and membrane-based desalination technologies can be integrated with renewable energy technologies, the amount of the produced water, the capacity of the system and the economic parameters of the yield water varies significantly for the systems. Table 7 summarizes the production capacity, energy demand and water production costs of RO and thermal desalination combined with renewable energy.

According to Table 7, photovoltaic utilizing processes are the most costly technologies in comparison with ordinary powered units. That is because the operation and maintenance costs of the batteries of this type are fairly high by the date. However, the environmental benefits of the renewable systems should be also mentioned. On the other hand, membrane technologies say RO as the pioneer, well-matured one saves considerably greater amounts of financial resources in comparison with other technologies. Thus, it can be easily understood why most of the researchers have focused their interest on RO and MED which is much cheaper than MSF among thermal systems. However, the high energy demand of MED makes it also impossible to use the systems under high energy deficit conditions.

Based on the summarized results in Table 7 which are obtained from the literature, RO technology is suitable for both small and large scale cases because of the flexible operating capacity. Indirect renewable technologies own more cases with large capacity demand. That can be explained for the reliability necessities of the consumers of large scale in addition to the economic concerns. In general, researches are directed to considering the long-term pros and cons of the technologies as well the initial investment and operating costs, considering the environmental objectives besides the eco-

Table 6. Main characteristics of direct solar desalination technologies

Process	Highlights	Water production	Description
Single-effect, single and double slop basin solar still	In cold climate, SSBSS works better than double slope stills. The opposite is true in warm climates. Double-basin type stills produce about 56% higher yield than single effect stills	4-5 L/m^2/d	-
Wick, basin and diffusion still	The wick can be tilted so that the effective area increases. Less feed water is in the still at any time in comparison to basin stills so the water is heated more quickly and to a higher temperature.	11 L/m^2/d	Per 1 m^2 active cross-section, 4 m^2 surface of evaporator and condenser, and energy input of 2.0 kWm^{-2}.
Multiple effect solar still	The condensation latent heat is reused so the efficiency increases. MESS has highest capital and operating costs among solar still desalination technologies.	15 L/m^2/d	for a value of 4.8 kWh/m^2/day of solar radiation.
HDH	HDH avoids direct contact of saline water with the collector that may corrode the still. HDH provides a means for low pressure, low temperature desalination and is the most cost competitive after RO and MSF.	4-12 L/m^2/d	GOR varies between 1.2 and 4.5
Solar chimney desalination	Solar chimney produces more water than solar stills but has higher maintenance costs.	-	-
Membrane distillation	MD is not commercialized yet. However, the low grade temperature allows the integration of the process with various systems.	-	-

Table 7. Comparison between thermal and membrane-based desalination technologies [134,198]

RE-desalination process	Typical capacity (m^3/day)	Energy demand (kWhe/m^3)	Water production cost (US$/$m^3$)
Solar still	<100	Solar passive	1.3-6.5
Solar MEH	1-100	Thermal: 29.6	2.6-6.5
		Electrical: 1.5	
Solar MD	0.15-10	45-59	10.5-19.5
Solar pond/MED	20,000-200,000	Thermal: 12.4-24.1	0.71-0.89
		Electrical: 2-3	
Solar pond/RO	20,000-200,000	Seawater: 4-6	0.66-0.77
		Brackish water: 1.5-4	
Solar CSP/MED	>5,000	Thermal: 12.4-24.1	2.4-2.8
		Electrical: 2-3	
Solar PV/RO	<100	Seawater: 4-6	11.7-15.6
		Brackish water: 1.5-4	6.5-9.1
Solar PV/EDR	<100	1.5-4	10.4-11.7
Wind/RO	50-2,000	Seawater: 4-6	6.6-9.0 small capacity
		Brackish water:1.5-4	1.95-5.2 for 1000 m^3/d
Wind/MVC	<100	7-12	5.2-7.8
Geothermal/MED	80	Thermal: 12.4-24.1	2-2.8
		Electrical: 2-3	
RO	10		4
Reverse osmosis	250		3.21
Reverse osmosis	100,000		0.43
RO-sea water	100,000-320,000		0.45-0.66
RO-sea water	15,000-60,000		0.48-1.62
RO-sea water	1,000-4,800		0.7-1.72
RO-brackish water	40,000		0.26-0.54
RO-brackish water	20-1,200		0.78-1.33
RO-brackish water	<20		0.56-12.99

nomics. Thus, it is expected that the thermal systems will be improved to satisfy the economic issues where the membrane base systems will be developed much on environmental aspects.

1-2. Indirect Solar Desalination

Solar energy can be used directly or indirectly for desalination. Systems that combine solar energy collection systems with conventional desalination technologies are known as indirect systems. In indirect systems, solar energy can be utilized to generate the heat required for desalination and/or to generate electricity that is used to provide the electric power required for conventional desalination plants [13]. There are several non-membrane desalination systems. Multi-stage flash, multi-effect distillation, heat pump, passive and natural vacuum desalination, vapor compression desalination, and absorption desalination systems combined with solar energy are described in the following sections [71,72].

1-2-1. Solar Assisted Multi-stage Flash (MSF)

Solar assisted multi-stage flash (MSF) systems offer the second largest installed desalination capacity after (RO) systems. A MSF desalination plant integrated with solar pond and partially powered by commercial electricity is more economical than any other type of solar powered desalination technology [73]. Most of the energy consumption in MSF plants is due to the thermal energy used to distill water, while some electricity is needed for pumping.

Fig. 27 shows that the temperature of feed saline water increases to saturation temperature due to heating by the brine heater unit and flashes in the vessel, where the pressure drops due to the vacuum pump. The brine flashed in each stage is discharged from previous stages. The vapor formed in each stage is condensed while the inlet saline water is preheated [46].

Singh and Sharma [74] reported that solar MSF units are superior to direct thermal desalination units using solar energy. The performance ratio (PR) of a solar multistage flash desalination unit was 3-10 times higher than that of a solar still. On the other hand, for the same plant capacity the water production cost and capital investment required for a multistage flash plant was lower than that for a solar still [74].

Solar MSF is especially useful given certain project requirements. For instance, a 10 m^3/d capacity solar powered multi-stage flash desalination plant with brine recirculation was developed by Mexico and the Federal Republic of Germany in 1974. This project's goal was to demonstrate the feasibility of solar energy as a source of thermic energy required for the MSF process. Similar desalination units were developed by the Swiss Federal Institute of Technology and Atlantis Energy, Ltd. and tested in Kuwait, where the results were found to be satisfactory [75].

Numerous studies have been performed to improve the efficiency of solar MSF. Szacsvay et al. [76] found that the water production costs of MSF units could be decreased by increasing plant

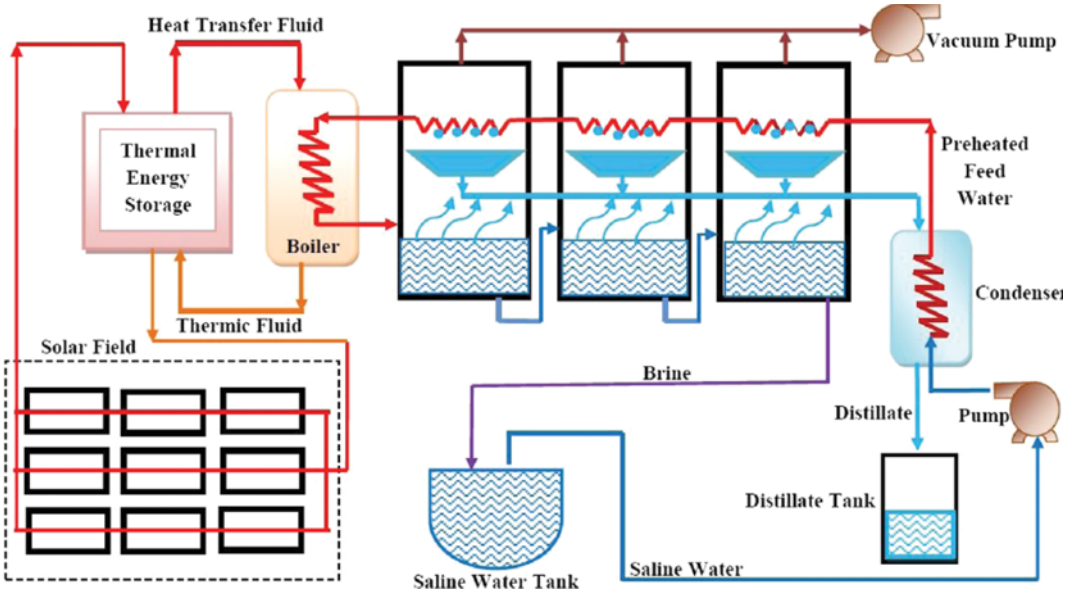

Fig. 27. Schematic representation of a solar powered multi-stage flash desalination system [77].

capacity and coupling the desalination unit with a solar pond, where collection and storage of solar energy would both occur [76]. The distillate yield of the plant could be increased by increasing the temperature difference between the hot brine and inlet seawater. The thermal storage subsystem was useful for leveling the thermal energy supply and allowing the production of desalinated water to continue during periods of low radiation and at nighttime [77]. Hanafi [78] performed a transient analysis of solar multistage flash desalination units and confirmed that the production of water could be increased by using water as heat transfer fluid in solar collectors and by increasing the number of storage tanks and their volume [78]. Laboratory prototype experiments by Safi [79] indicated that almost 15 m^3/d of water could be produced by coupling ten flash desalination units of 1 m^2 area each operating at 0.9 bar with solar pond of 70 °C. The desalination unit was coupled to a 1,500 m^2 solar pond for tests [79]. The gained output ratio of solar MSF desalination units could also be increased by operating the plant along a wide temperature range, as well as discharging the condensate during the last stage. Lu et al. [80] reported that zero discharge desalination could be achieved by integrating MSF desalination units with solar ponds and brine concentration recovery systems (BCRS), such that the rejected brine could be converted into salt and used for maintaining the salinity of solar ponds. These conclusions were drawn from 16-year stud-

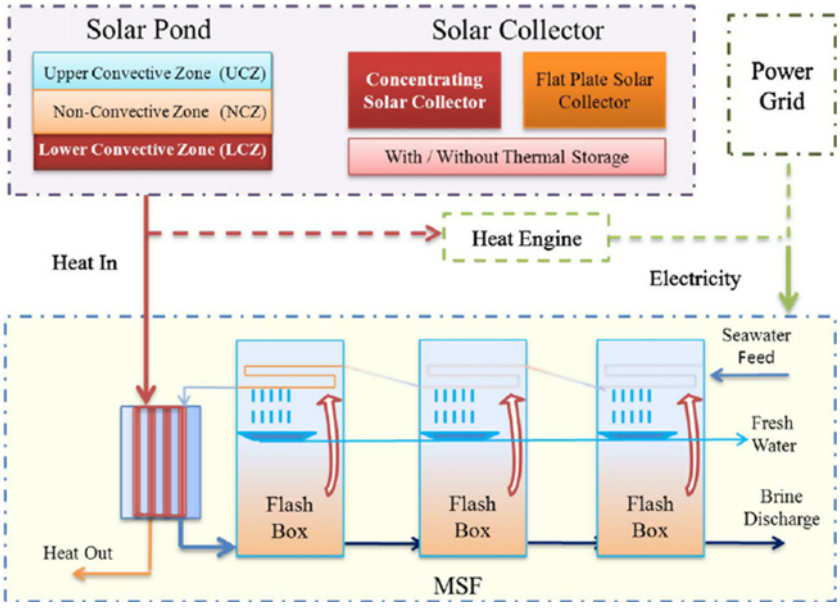

Fig. 28. Schematic of a solar pond assisted multi-stage flash desalination process [87].

ies of the El-Paso solar pond [80].

1-2-1-1. Solar Pond Driven MSF Desalination

As illustrated in Fig. 28, a solar pond (SP) is a stable pool full of salt water. There is a non-convective layer in the middle, where the water salinity increases from top to the bottom. A gradient is maintained so that convective mixing of absorbing solar radiation and subsequent increases in temperature may be prevented. Heat is passively collected and stored in the lower convective zone (LCZ), because it is impossible for heat to pass the non-convective zone (NCZ). Most commercial MSF units operate with top brine temperatures of 90-110 °C [81] and are heated by steam, while solar pond systems operate in the range of 30-95 °C. Note that in solar pond-assisted MSF systems, unlike conventional MSF units, the first stage of the MSF heat exchangers is a liquid-liquid heat exchanger instead of a steam-liquid heat exchanger. Energy requirements sometimes dominate other effective factors in both design and practice. However, solar pond units have reasonable product costs in comparison with nuclear reactors and other sources in areas with small populations [82]. Cogeneration plays another important role in solar ponds where SP units can store extra waste heat, such as heat from gas turbine exhaust harvested during peak times to lower water production costs and decrease solar pond size. Increase of the power plant from 30 MWe to 120 MWe leads water production quantities to increase from 303 to 1,816 m^3/day [83]. Thus, solar ponds have many advantages over other solar desalination technologies [84], such as low cost per unit area of the collector, inherent storage capacity, and capability of utilizing reject brine, which is often considered a waste product. There is also the potential of low temperature surface water to be used as cooling water in hot weather [85,86]. However, there are several disadvantages of these systems, such as the requirement that solar ponds have sunny conditions, large flat land areas, and serious environmental impacts such as soil contamination by pond brine leakage if the leakage is not monitored carefully. It is also important to maintain the salinity profile of the solar pond, the saline water needs to be maintained at low pH, pond clarity must be monitored very carefully, and wind factors must be considered before construction [87].

1-2-1-2. Solar Collector Driven MSF

Some researchers have concluded that concentrating solar power (CSP) offers a sustainable alternative to fossil fuels for large scale seawater desalination [88]. In SCP, a solar collector field is connected to a conventional distillation plant to provide thermal energy for the desalination process because fossil fuel is not economical or sustainable for long-term use in large scale desalination units. The collectors are usually tracked as stationary, single-axis, and double-axis groups. Stationary collectors usually run in a wide range from 30° to 240 °C with concentration ratios of 1-5, while the single-axis type shows a greater concentration ratio from 5 to 50 while operating from 60°-300 °C. Double-axis collectors are operated from 100°-2,000 °C with concentration ratios varying from 100 to 1,500 [89].

As mentioned, solar collectors work under a wide range of temperatures, so they should be chosen based on the desired process temperature. Concentrating solar systems can be trough, dish, or central receiver tower types. The possibility of conjunctions with large heat facilities makes concentrating solar systems superior to other renewable sources. It is also practical to use these systems in hybrid mode with fossil fuel or biomass to compensate for fluctuations in daily irradiance and to produce electricity beyond the sunshine hours [90]. Fig. 29 illustrates different solar technologies.

Studies have already been performed for MSF process optimi-

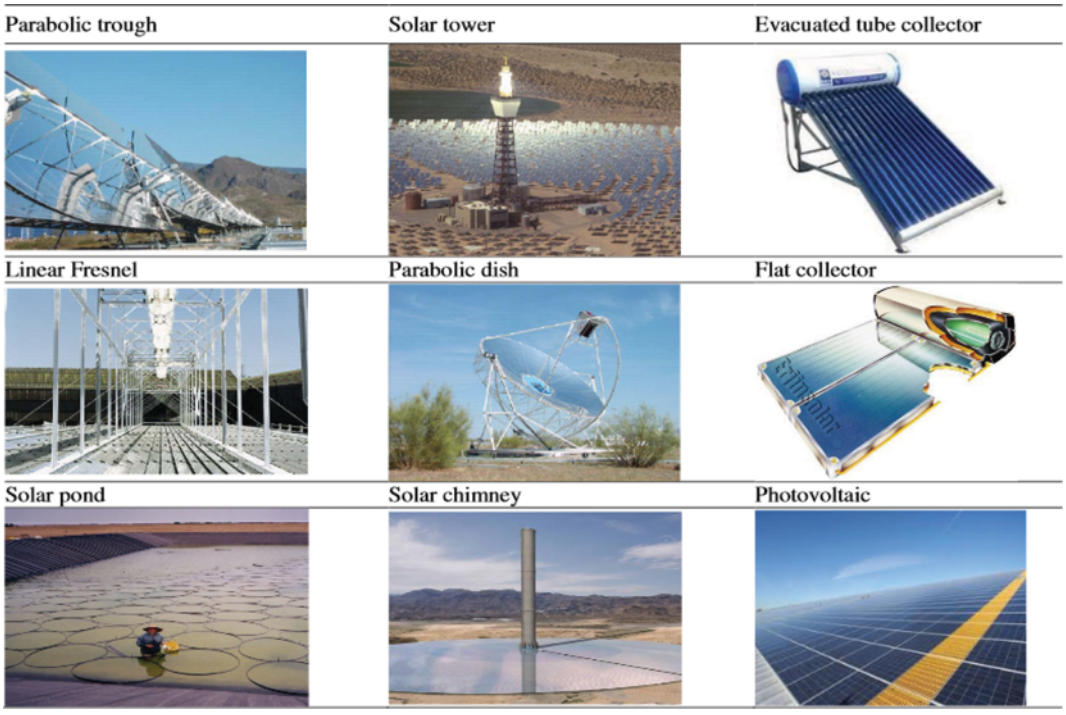

Fig. 29. Different solar technologies [99].

zation. Shaobo et al. [91] used pinch analysis to optimize a solar multi-stage flash (MSF) desalination process and concluded that a wide working temperature range of MSF is needed to enhance performance. In addition, to gain higher gained output ratio, they found that it is better to discharge the brine at the last stage. It is also important to control the flash evaporation pressure; by reducing the flash evaporation pressure from 0.014 MPa to 0.010 MPa, the desalination rate could be increased almost five-fold in some direct solar thermal desalination systems [92]. Since solar heat is intermittent, an effective thermal storage system, i.e., a storage tank, can be used for thermal buffering [93]. MSF uses the seawater feed as the coolant, which means that MSF uses sensible heat to recover the latent heat from the distilled water. This is why MSF requires large amounts of seawater recirculating within the system and consumes more electricity than MED processes. In addition, MED plants are more flexible to operate under partial loads.

1-2-2. Solar Multi Effect Distillation (MED)

As illustrated in Fig. 30, multi-effect distillation (MED) units consist of vessels known as effects that are maintained successively at low pressure, where saline water is sprayed. The necessary heat for evaporation in the first effect is supplied by an energy source that can be solar energy or fossil fuel combustion. Thus, the vapors formed are used to heat the feed in the next effect. The latent heat of the vapors produced in the previous effects is utilized for the following effects in MED. MED systems are gaining market share due to better compatibility with solar thermal desalination, lower sensitivity to scaling, and greater suitability for limited capacity applications [94]. A dynamic computer model developed by Tsilingiris [95] showed that an MED unit coupled to a solar pond 30,000-40,000 m^2 in area could annually produce 1,00,000 tons of distilled water at a cost comparable to conventional methods of desalination in which water production cost mainly depends on the cost of salt. The cost of production in an MED also decreases with increases in solar pond area [95].

MED units show good flexibility when compared with other systems. For instance, the essential power of a double effect Li-Br absorption heat pump can be provided by a solar collector field, as shown in Fig. 30. The heat pump is coupled to the MED so that it uses the heat from the solar field and the MED unit uses the heat rejected by the condenser and absorber of the heat pump. The thermal energy consumption and solar field requirement for MED units coupled with absorption heat pumps are half those of a conventional MED system. Such systems can be operated in hybrid solar/gas mode, solar mode, or even gas mode, with performance ratios ranging from 10 to 20 [97].

The feasibility of low temperature MED (LT-MED) units integrated with flash chambers and solar collectors was studied by Jiang et al. [92], who described the performance of a directly heated solar desalination system. The design concept was based on a direct solar energy collection unit integrated with flash evaporation and low temperature multi-effect distillation (LT-MED) equipment. The water heated in the solar collector was flashed in the flash chamber, and the vapors produced were used as a heating source for the first stage of MED. The water discharged from the flash chamber was used as the feed water of the MED unit. Replacing the condenser of a solar operated power plant with an LT-MED unit is more efficient than using an LT-MED fed by the exhaust steam of a solar operated power plant compressed by a thermal vapor compressing unit [98]. Sharaf et al. [1] investigated two configurations for integrating MED with solar cycles. In the

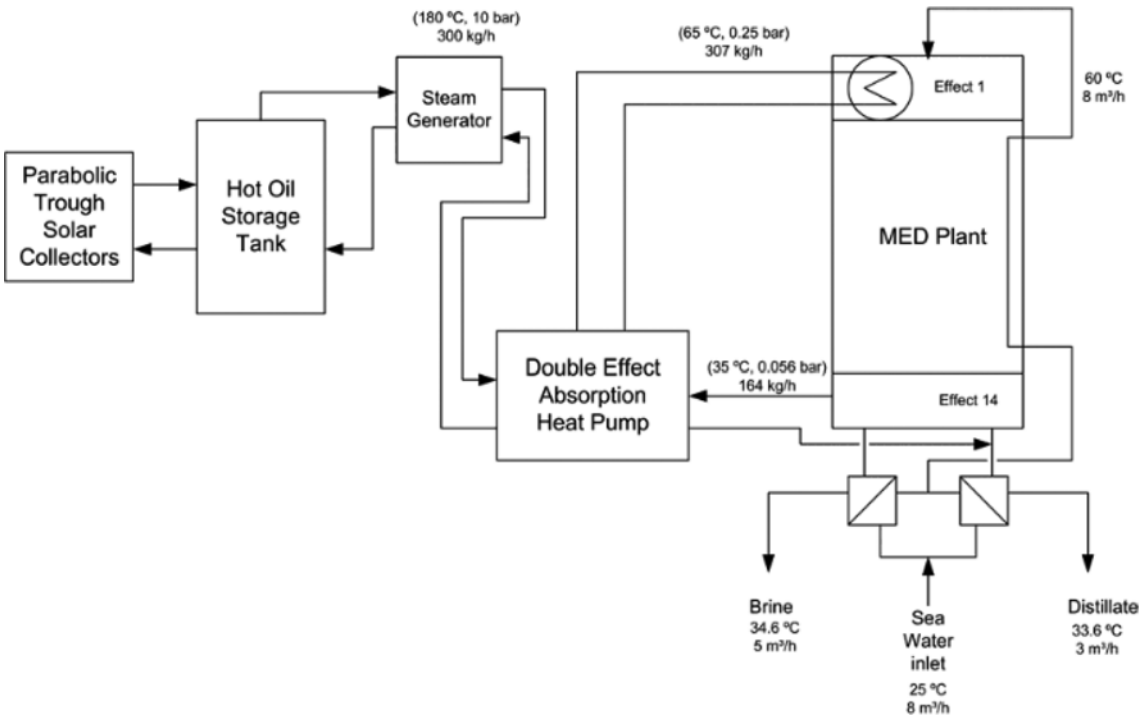

Fig. 30. Schematic representation of an improved MED system [96].

first technique, solar energy was directly transferred from the solar collector field via an evaporator heat exchanger for use in the first effect of the MED process. In the second technique, the energy exhausted from the organic Rankine cycle (ORC) turbine was used in the first effect of the MED process. The second technique produces electricity in addition to desalted water. Parallel feed configuration dominated against the forward feed when there was a feed heater configuration, while increasing the number of effects to more than 12 effects.

Different configurations are available, such as multi effect distillation-backward feed (MED-BF), multi effect distillation-parallel feed (MED-PF), multi effect distillation-forward feed with heater (MED-FFH), and multi effect distillation-forward feed (MED-FF), but MED-FFH and MED-PF are found to be more efficient than all of these [1]. The SORC-Ejector-MED unit is capable of treating high saline water with an exergy efficiency of 40%. This system is driven by low-grade heat sources such as solar energy and combines a supercritical organic Rankine cycle (SORC), an ejector, and a multi-effect distillation (MED) desalination system. It can be used for treating seawater or concentrated brine [99]. The gain output ratio (GOR) of the MED unit depends mainly on the evaporator temperature of the last effect and is much less affected by the temperature of the feed stream. The results indicate that effect number is very important to balance lower costs and more highly distillated products in the MED system, because degree of distillation is related to the number of effects. [100]. Joo and Kwak [101] developed a solar MED unit with 3 m^3/d capacity and a shell and tube type heat exchanger, which was optimized for solar thermal desalination systems. They concluded that multi-effect distillation required about 40 kW heat and a 35 kW cooling source to produce 3 m^3/day of fresh water. The solar assisted MED process requires both thermal and mechanical energy, like the solar assisted MSF process. However, MED systems may be operated in three configurations: forward feed, backward feed, and parallel feed [101].

MED systems use falling film horizontal tube evaporator/condensers to achieve high heat transfer efficiency [102], and operate with a relatively low top brine temperature (usually less than 75 °C) to reduce scale formation and corrosion. The high purity of the water produced also allows the water to be used directly for industrial processes (as boiler feed water) or to be blended with locally available brackish water [103]. MED systems can be combined with heat pumps to improve overall efficiency [104,105]. The combination of low cost and low energy consumption, together with the inherent durability of low temperature MED systems, avoids the necessity of comprehensive seawater pretreatment and makes the MED process one of the best candidates for safe and durable large capacity desalination [106]. MED has higher overall efficiency, higher heat transfer coefficient, more independent stages, and requires less water recycling than MSF [107]. However, to decrease energy consumption, MED systems require large flat areas for evaporators to reduce the temperature differences between adjacent stages. [108].

1-2-2-1. Solar Pond-assisted MED

A solar pond-assisted MED system is similar to a solar pond-driven MSF system, but the lower temperature requirements of MED make solar pond operation easier than in MSF. Using mathematical modeling, Hawaj and Darwish [109] found that intermediate steam temperatures (80-90 °C) are more efficient than higher temperatures for the operation of solar-assisted MED systems, because higher steam supply temperatures decrease solar enhancement. Large ratios of solar pond surface area to MED heat transfer area leads to continuous increases in pond temperature [109]. Garman and Muntasser [110] found a linear relationship between the thermal load required for the desalination unit and the surface area of the solar pond. They suggested that the optimum thickness for the upper convecting zone is 0.3 m, while for the non-convecting zone it is 1.1 and for the lower convecting zone it is 4 m.

Solar collector-assisted MED seawater desalination processes have been studied extensively. Some solar MED systems have been combined with heat pumps to improve efficiency. The technical reliability of solar collector-assisted MED systems has been validated by long-term tests. Two well-known experimental units are the Abu Dhabi solar desalination plant and the Solar Thermal Desalination (STD) Project [111-113] at the Platform a Solar de Almeria (PSA), Spain. The Abu Dhabi solar desalination plant, which operated from1984 to 2002, was equipped with evacuated tube solar collector (ETC)-assisted MED systems [111]. Like other fluid dealing processes, some plant maintenance is necessary, such as removal of dust deposition that could cause monthly drops in glass tube transmittance of 10-18%. Such transmittance deficiencies could lead to drops in water production to 40% of clean collector production [114].

Economic feasibility studies [115] indicate that operating desalination systems solely on solar energy is not feasible, because of the high percentage of inactive time. The use of an integrated collector storage (ICS) system is recommended in this paper [116]. The use of a double heat pump improves the performance of solar thermal technology as shown by a 14 stage MED. These results were taken from a two-phase project conducted in Spain [116].

Desalination HP units are generally used for small and medium scale [117] applications and are normally combined with other thermal processes. Heat pump combined systems run in a similar fashion. All recover low temperature vapor from parts of the MED or MSF system and convert it to higher temperature vapor to improve system efficiency. The whole desalination system requires less cooling water and consumes less electricity because the low temperature vapor is recovered [87].

Applications of heat pumps in desalination systems include thermal vapor compressor (TVC) (Fig. 31(a)), mechanical vapor compressor (MVC) (Fig. 31(b)), absorption heat pump (ABHP) (Fig. 31(c)), and adsorption heat pump (ADHP) (Fig. 5(d)) [118]. There are additional differences between heat pump-based systems illustrated in Fig. 6: (1) MVCs use electricity as an energy source and can function as stand-alone desalination systems; (2) TVCs use higher temperature and pressure (4,200 kPa) steam; and (3) ABHP and ADHP use either higher temperature steam or other heat sources [87]. As can be seen in Fig. 32, MSF systems can be connected with a solar thermal heat source and the power grid at the same time, or can be connected with a solar thermal system through a heat engine to provide heat and electricity at the same time. Solar pond type solar thermal systems may be especially

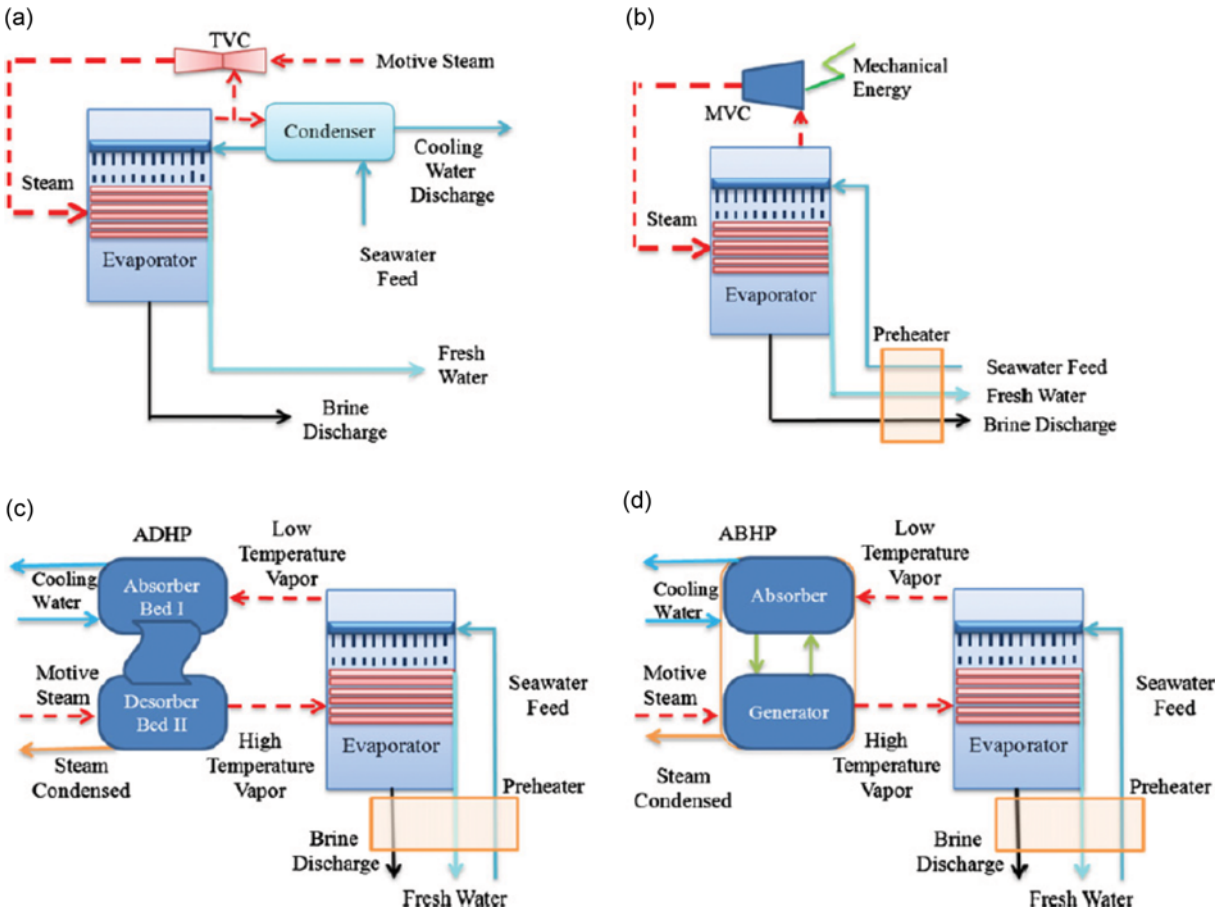

Fig. 31. Possible configurations for solar assisted heat pumps and combinations [156].

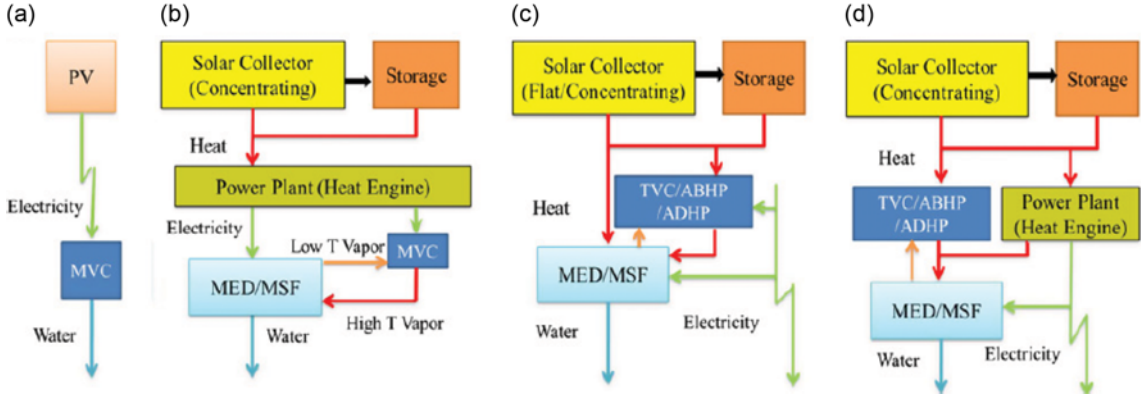

Fig. 32. Schematic of different heat pumps used in desalination. (a) Thermal vapor compression (TVC), (b) single effect mechanical vapor compression (MVC), (c) single effect adsorption heat pump, and (d) single-effect absorption heat pump [156].

applicable, since the salt produced could be used in the pond itself [73,87].

A mechanical vapor compressor (MVC) or thermos vapor compressor (TVC) is necessary to increase the pressure and temperature of vapor in vapor compression desalination systems. Seawater is used as the feed and is heated by an external heat source until it flashes. The compressed vapor is then used to heat the same stage or the inlet feed water of the other stages.

Helal and Al-Malek [119] developed a mechanical vapor compression desalination unit with 120 m^3/d capacity that was powered by PV/diesel and included heat recovery [119]. The hybrid system was capable of reducing emissions by 179 tons of CO^2 per year, but the water production cost was high compared to conventional methods. They found that increasing plant capacity reduced the costs.

Mechanical vapor compressor (MVC) desalination units driven

by wind/PV hybrid system consist of MVC, PV module, wind turbine, and storage tank. The hybrid unit supplies power to the desalination system and is connected to an external electrical network in case of deficiencies. Excess power is stored and the remaining power is supplied to the external electrical network. Three different locations in Morocco were used to validate the theoretical system. The cost of water production by this method is comparable to that of conventional water production methods if the capacity is greater than 120 m^3/d [120].

Specific power consumption, steam flow rate, and total water production costs of multi-effect distillation-parallel feed-thermo vapor compressor (MED-PF-TVC) units are lower than those of multi effect distillation-parallel feed-mechanical vapor compressor (MED-PF-MVC) units. MED-PF-MVC is competitive if there are more than 12 effects. Reductions in the value of the compression ratio associated with increases in evaporator numbers result in decreases of specific power consumption, solar field area, and thermo-economic costs. The operation of a steam ejector increases the gain ratio in a straightforward manner [121].

Results of research on multi-effect thermal vapor compression (ME-TVC) [122] showed that the maximum gain ratio varied between 8.5 and 18.5, respectively, for systems with 4 and 12 effects and that the optimal top brine temperature ranged between 55.8 and 67.5 °C with a reasonable specific heat transfer area. The optimal ranges of compression and entrainment ratios are between 1.81 to 3.68 and 0.73 to 1.65, respectively. The optimal results for a 4-effect TVC unit were also compared with those of three commercial four-effect units having almost the same input. These comparisons showed that further improvements in distillate output production, compression, and entrainment ratio can be achieved by combining an ME-TVC system with a conventional multi-effect unit [122].

TVC has been studied in combination with MED or MSF for use in different sizes of commercial desalination plants [123] in which steam compression is carried out by an ejector, and the vapor from the last effect of the MED process is carried back to the first effect by a motive stream. MVC is widely used for its simplicity and relatively low energy consumption. The performance of MVD is better when there is lower concentration and increased compressor speed. The highest average performance ratio obtained by Bahar et al. was 2.52 [124]. ABHP and ADHP are regarded as having higher potential for desalination applications than TVC and MVC. ABHP and ADHP processes were studied with an open cycle using zeolite as the solid vapor adsorbent [125], but no commercial applications have been reported.

1-2-3. Solar Vacuum Desalination

It is possible to produce vapor from saline water at lower temperatures by creating a vacuum. A vacuum can be created by vacuum pumps or, naturally, by gravity. Vacuum pumps are power consumers, while natural vacuums simply require the fall of water under gravity [126].

1-2-3-1. Solar-assisted Passive Vacuum Desalination (PVD)

Al-Kharabsheh and Goswami adopted a process for small scale desalination applications that used a thermal system without a steam ejector or vacuum pump. Such systems are known as passive vacuum pump (PVD) systems [127,128].

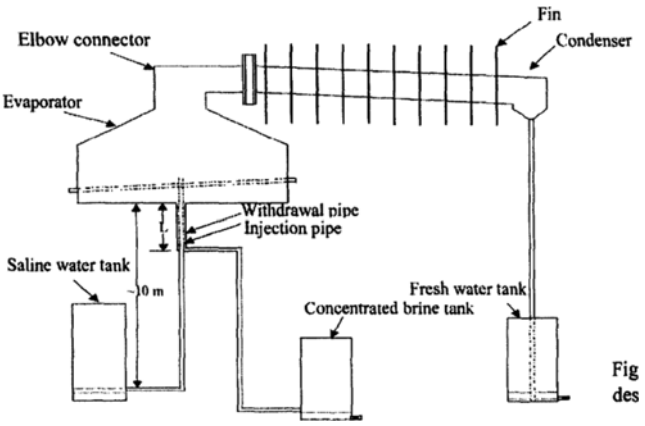

Fig. 33. Schematic of passive vacuum flash desalination [128].

As shown in Fig. 33, the seawater initially filling a thermal system is more than 10 m above the ground, and then the water drains to generate a vacuum in the head space created when the standing column of water held by atmospheric pressure drops by gravity force in a sealed tank that is taller than 10 m.

In Abutayeh and Goswami's model [129], the simulated process consists of pumping seawater through a solar heater before flashing it under a passively created vacuum in an elevated chamber. The vacuum causes evaporation and balances the hydrostatic pressure inside the chamber and the atmospheric pressure. Several different passive vacuum systems have been combined with sensible heat thermal energy storage (TES) [130], wind power [131], and PV systems [132]. Passive vacuum units generate a vacuum using natural gravity without any hydraulic pressure sources such as vacuum pumps. Therefore, non-condensable gases accumulate over time within seawater and disrupt the vacuum conditions in the evaporator, resulting in decreases in overall heat transfer efficiency and fresh water production rate [46].

In conclusion, PVD is a simplified MSF/MED thermal system that is most suitable for applications in contexts such as ships, where the deck is more than 10 m higher than sea level and where strong desalination systems are needed.

1-2-3-2. Natural Vacuum Desalination Systems

It has been repeatedly emphasized that natural vacuum desalination systems are suitable for small scale applications. Al-Karabsheh and Goswami [133] did theoretical analyses and obtained preliminary experimental results using natural means of producing vacuums such as gravity and atmospheric pressure. They found that the vacuum equivalent of 4 kPa (abs) or less could be obtained depending on the ambient temperature at which condensation takes place. Fig. 34 schematically represents such facilities.

A system recently developed by Gude et al. is capable of producing 100 L/d freshwater using a solar collector 18 m^2 in area while considering climate fluctuations. This unit was equipped with a thermal energy storage volume of 3 m^3 [134].

An innovative solar-driven flash desalination system was proposed by Maroo and Goswami [126]. This system uses the natural force of gravity and atmospheric pressure to create a vacuum and consists of evaporator(s), condenser(s), collection tanks, a heat source, and a seawater circulation pump. A theoretical analysis of

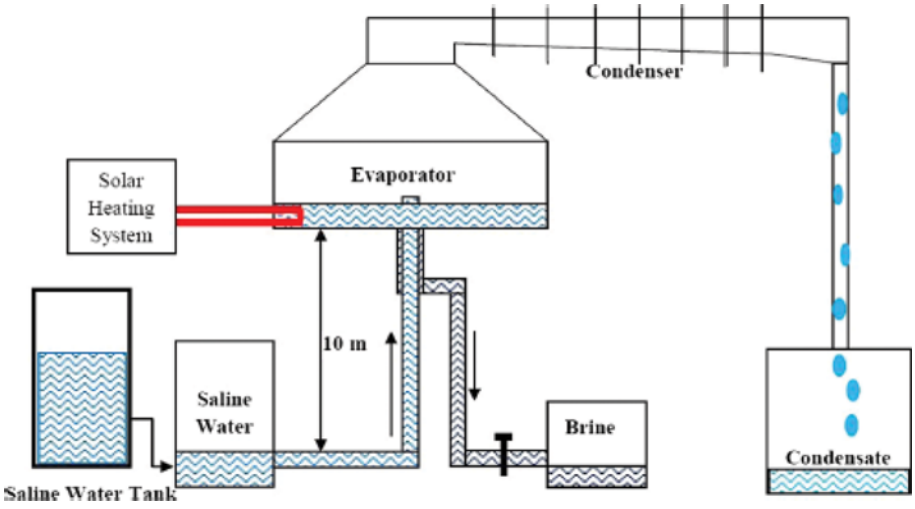

Fig. 34. Schematic representation of a natural vacuum desalination system [133].

the single-stage and two-stage concepts was performed for the system coupled with a constant temperature heat source and solar collector. When coupled with a solar collector 1 m^2 in area, a single-stage system produces 5.54 kg of water in 7.83 h, while a two-stage system produces 8.66 kg in 7.7 h. The performance ratios including the efficiency of the solar collectors were 0.48 and 0.75 for a single-stage and two-stage system, respectively, or 0.748 and 1.350 if only the useful heat collected by the solar collector is considered. It is also possible to couple natural vacuum desalination systems with absorption refrigerators. Using a thermal storage system with the combined system, the cooling capacity is 3.25 kW while the distillate yield is 4.5 kg/h [135].

The results of a field test of a two-stage low temperature phase change desalination process indicate that a two-stage desalination process has a specific energy consumption of 1,500 kJ/kg of freshwater. Economic analyses conducted of this desalination system suggest desalination costs of \$3/m^3 when using a cheap waste heat source purchased at \$0.5/GJ. The desalination costs would be less than \$7/m^3 if powered by a low grade flat plate solar collector heat source [136]. Ayhan and Al Madani [131] developed a novel desalination system using natural vacuums to meet water requirements in a sustainable manner. Their system consists of an evaporator column exposed to solar radiation. Zhao and Liu [227] proposed an innovative solar multi-effect evaporator-condenser desalination system in which the vacuum is maintained by tides. Stable operation of the unit can be achieved for areas with tides that range 2 m in height.

1-2-4. Adsorption Desalination

As seen in Fig. 35, the main units comprising an adsorption desalination system are as follows: evaporator, adsorption beds,

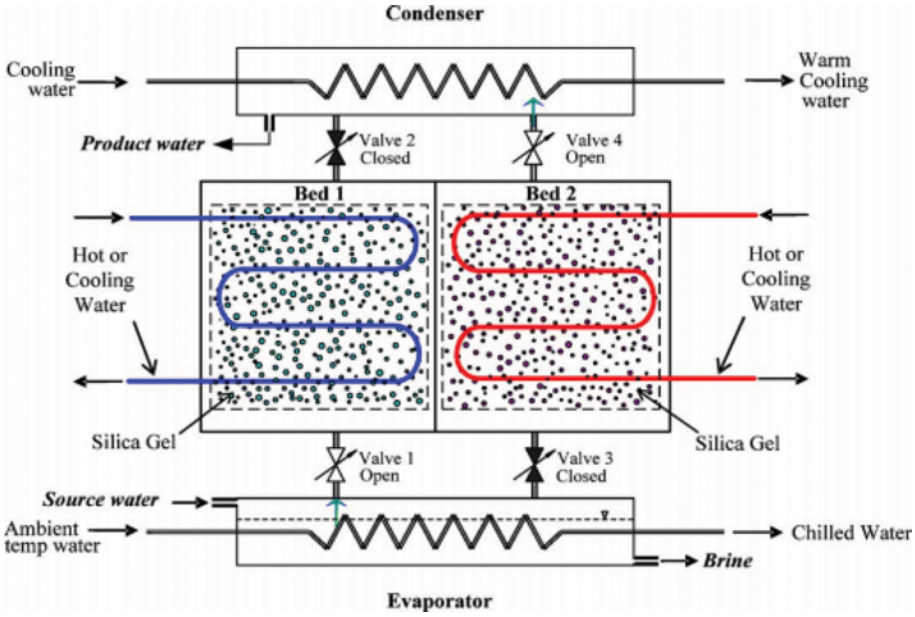

Fig. 35. Schematic representation of a two bed adsorption desalination system [137].

and condenser. For a single bed system, the adsorption occurs in a single bed, whereas for a two-bed system, adsorption takes place in one bed and desorption simultaneously takes place in another bed [137]. Saline water evaporates in the evaporator and is adsorbed by a bed (or beds) maintained at low temperature by circulating cooling water.

The water production rate and energy consumption of an adsorption desalination system are mainly dependent on the cooling water inlet and hot water inlet temperatures, as well as the silica gel adsorption constant. Such systems can be optimized for high water production rate with low energy consumption only when the plant is operating under optimum conditions [137]. Zejli et al. [125] studied solar adsorption desalination in combination with a multi-effect distillation system using theoretical models. The proposed system consists of an evaporator set between two reactors filled with zeolite as adsorbent material the adsorbent heat required for the process was supplied by solar parabolic trough collectors. The vapors leaving the adsorption system transferred the heat required by the three effect distillation system. The saline water entering the condenser of the three effect distillation unit was preheated to 70 °C by the heat transfer fluid and allowed to flash inside the evaporator, where the necessary vapor was produced. In the meantime, during the first cycle one adsorbent bed runs at 120 °C while the other runs at 195 °C. In the second cycle, the adsorbent bed temperature is reversed by changing the direction of flow of the hot fluid. The vapors produced are adsorbed by the low temperature zeolite bed, and the adsorbed water vapor is released by passing hot heat transfer fluid through the bed. Vapor is used as the heat source for the three effect distillation system to evaporate brine water that is disposed by the evaporator, and the vapors thus formed are then condensed.

Wu et al. [138] analyzed the potential of adsorption desalination systems to use waste heat to co-generate cooling and fresh water from saline water through adsorption on silica. They focused on thermodynamic cycles for the adsorption desalination system. The optimum situation, in which was obtained maximum water production with minimum energy consumption, occurred if the evaporator temperature was kept equal to or higher than the temperature of the cooling water used to cool the adsorption bed. The proposed thermodynamic models were experimentally verified, and the results were found to be close to the predicted values [139]. The daily water productivity of four bed adsorption desalination facilities operating with silica gel and low temperature waste heat was 4.7 kg/kg. Water productivity can be enhanced by manipulating temperature, for example by increasing the temperature of chilled water supplied to the evaporator and decreasing the temperature of cooling water circulated around the constant hot water inlet to the adsorption bed.

Thu et al. [140] sought to optimize AD cycles according to performance parameters such as specific daily water production (SDWP), cycle time, performance ratio (PR) for various heat source temperatures, mass flow rates, and cycle times along with a fixed heat sink temperature. The maximum potable water production per ton of silica gel adsorbent per day is about 10 m^3, while the corresponding performance ratio is 0.61. They found that longer cycle time is required to achieve maximum water production at lower heat source temperatures. Ng et al. [141] studied the performance of a waste heat-driven adsorption desalination cycle producing potable water and refrigeration using mathematical models. They validated their system through experiments under different operating parameters. The system was successfully operating at a hot water inlet temperature of 65 °C. An advanced adsorption desalination system was developed by Thu et al. [142], which utilized the heat rejected by the condenser to evaporate saline water from the evaporator. Improved yield was obtained at high hot water inlet temperatures, low cooling water temperatures, and by main-

Table 8. Main characteristics of indirect solar desalination technologies

Process	Highlights	Water production	Description
Solar assisted multi-stage flash	A Solar assisted MSF desalination plant integrated with solar pond is the most economical desalination technology. PR of a solar MSF is 3-10 times higher than that of a solar still. Solar ponds need sunny conditions, large flat land areas, and serious environmental impacts such as soil contamination by pond brine leakage.	12-15 L/m^2/d	By coupling 10 flash units operating at 0.9 bar with solar pond of 70o c.
Solar multi effect distillation	MED systems are low cost and low energy consumers with the inherent durability of low temperature. MED does not require comprehensive seawater pretreatment so it is used for large capacity desalination. In order to decrease energy consumption, MED systems require large flat areas for evaporators to reduce the temperature differences between adjacent stages.	6-13 L/m^2/d	MED unit 30,000-40,000 m^2 in area could annually produce 1,00,000 tons of water at a cost comparable to conventional methods of desalination
Solar assisted heat pump	HP units are generally used for small and medium scale applications and are normally combined with other thermal processes.	-	-
Solar vacuum desalination	Most suitable for applications in contexts such as ships, where the deck is more than 10 m higher than sea level and where strong desalination systems are needed.	17-27 L/m^2/d	Both single-stage and two-stage systems are possible

taining high flow rates. The optimum cycle time of this advanced adsorption desalination system was found to be shorter than that of a conventional adsorption desalination system.

The main characteristics of indirect solar desalination technologies are summarized in Table 8.

2. Non-solar Desalination Systems

Although non-solar energy sources are not considered promising thermal resources for desalination processes, several studies have examined integrated wind, geothermal, and waste heat units used by desalination systems.

2-1. Geothermal Energy in Thermal Desalination

Geothermal energy is a proven technology for electricity production, but is most often used only on small research scales. Geothermal energy is useful for desalination due to the following advantages:

1. Stability: Geothermal energy provides a reliable heat supply, ensuring the stability of thermal desalination.

2. Maturity: Geothermal production technology (the extraction of hot water from underground aquifers) is mature.

3. Conformity: Typical geothermal source temperatures are in the range of 70-90 °C, which is ideal for low-temperature MED desalination.

4. Economical: Geothermal desalination is cost effective, and simultaneous electricity production is possible.

5. Environmental: Geothermal desalination is environmentally friendly, as only renewable energy is used with no emissions of air pollutants or greenhouse gasses [143].

High-temperature geothermal energy sources are mostly used to produce electricity, while low-temperature sources seem suitable for desalination. The advantage of geothermal sources is that energy output is generally constant, making them ideal for thermal desalination processes. Note that geothermal waters can be simultaneously used for two purposes in desalination processes, both as feed and heat transfer media for desalination [143]. Bourouni et al. [144] reported an aero-evapo-condensation process that was found to be promising for cooling as well as desalting geothermal water. A geothermal spring with a water temperature of about 70 °C was used in this study [144,145]. Karystsas [146] published a case study of a low enthalpy geothermal energy driven seawater desalination plant built on Milos Island in Greece that coupled MED units to a geothermal groundwater source with temperatures ranging from 75 to 90 °C. The exploitation of low enthalpy geothermal energy would save the equivalent of 5,000 TOE/year for a proposed plant with a capacity of 600-800 m^3/day of fresh water. Geothermal capacity is not a major factor in desalination processes such as MED, thermal vapor compression (TVC), single-stage flash distillation (SF), and MSF. These processes benefit greatly when coupled to geothermal sources because considerable amounts of energy are needed for pre-heating.

2-2. Wind Energy in Thermal Desalination

Wind energy is available in a variety of environmental contexts. Windy conditions at mountain stations, in coastal areas, and on islands are all suitable for wind-powered desalination systems. It is important to couple wind energy with appropriate processes for the operation of wind-powered desalination plants. These systems should not be sensitive to repeated start-up and shutdown caused by rapidly changing wind conditions. Wind energy is considered a mechanical energy source rather than a thermal energy source. Although there are several different desalination processes with varying degrees of technological maturity, only a few can utilize the electrical energy from a wind turbine and are technologically ready to be employed. Mechanical vapor compression has been widely studied in this context [143]. Mechanical vapor compression (MVC) processes are more tolerant of intermittent operation than RO, but are not traditionally used with variable power supplies [147]. However, two independent wind-driven MVC desalination plants that operate with variable power have been built. In both plants a variable speed compressor and a resistive heating element in the brine tank allow a variable amount of power to be absorbed by the unit [148]. One plant on Borkum Island in the Leer District in Lower Saxony, northwestern Germany uses a 60 kW wind turbine, an MVC unit with a 4-36 kW compressor, and a 0-15 kW resistive heater. The system is capable of producing distillate at 0.3-2 m^3/h and consumes 16-20 kWh/m^3 [149]. Another wind-powered MVC desalination plant with a capacity of 360 m^3/day is located on the Island of Rugen in the Baltic Sea [148]. The wind energy production capacity at this plant is 300 kW. Depending on wind speed conditions, distillate production varies between 2 and 15 m^3/h.

2-3. Waste Heat Energy in Thermal Desalination

As shown in Fig. 36, waste heat can be stored to be utilized for desalination. Lower thermal losses, lower operation costs, and lower maintenance and capital costs are major benefits of low temperature desalination. Studies of a low temperature desalination process that taps heat rejected from the condenser of a domestic air-conditioning system indicate that evaporation of saline

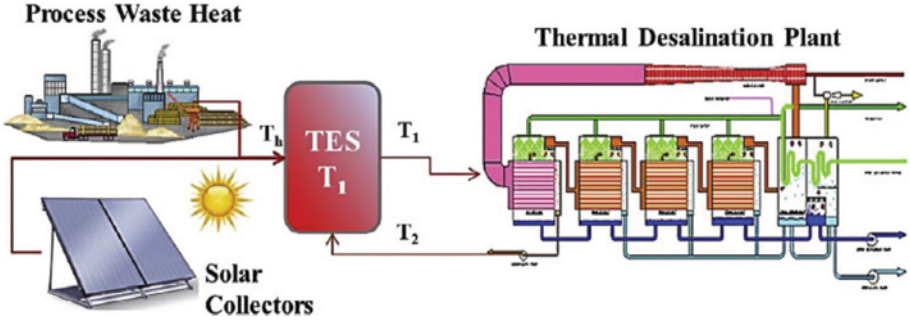

Fig. 36. Thermal desalination system powered by waste heat source [145].

Table 9. Main characteristics of non-solar desalination technologies

Process	Highlights	Water production	Description
Geothermal assisted desalination	Low-temperature sources seem suitable for desalination. Energy output is generally constant in Geothermal sources, which makes them ideal for thermal desalination processes.	-	-
Wind energy assisted desalination	Windy conditions at mountain stations, in coastal areas, and on islands are all suitable for wind-powered desalination systems. But these systems should not be sensitive to repeated start-up and shutdown caused by rapidly changing wind conditions.	6-13 $L/m^2/d$	The plant uses a 60 kW wind turbine, an MVC unit with a 4-36 kW compressor, and a 0-15 kW resistive heater.
Waste heat energy in thermal desalination	Lower thermal losses, lower operation costs, and lower maintenance and capital costs are major benefits of low temperature desalination.	-	-

water takes place at near-vacuum pressures created by exploiting the principles of local barometric head. The evaporator can be run in a temperature range from 40-50 °C with heat supplied by a TES unit. The energy requirements for the system are lower than those for an MSF distillation process. The thermal energy rejected by an absorption refrigeration system (ARS) with a cooling capacity of 3.25 kW (0.975 tons of refrigeration) along with an additional energy input of 208 kJ/kg of desalinated water is sufficient for desalinated water production at an average rate of 4.5 kg/h. This energy consumption is only 60% that of a typical MSF distillation process (338 kJ/kg) [150]. A TES unit volume of 10 m^3 and a solar panel area of 25 m^2 are required for such applications.

In another recent study [151], an integrated process model was developed for the novel application of a sensible TES system for energy conservation and water desalination in power plants. In this configuration, a cold TES was designed to diminish the negative effects of high ambient temperatures, which weaken the performance of air-cooled condensers. These condensers can successfully cool a 500 MW CCPP (combined cycle power plant). Stack gases from CCPP may also be used to drive an ARS, which maintains the chilled water temperature in a TES tank. A process model integrating CCPP, ARS, TES, and MED was developed to optimize the volume of the TES.

In many cases, the energy requirements for desalination process increase directly with thermal energy source temperatures due to higher heat losses to the ambient atmosphere. This suggests that low temperature operation, and thus low temperature TES systems, could be more energy-efficient as described above [134]. Part of the cooling load from the TES was utilized to cool the final condenser in the MED system, in order to facilitate additional stages in the MED process.

Further, when the number of stages increases, thermal energy requirements decrease. Preliminary analysis of the integrated process showed that a cold TES tank volume of 2,950 m^3 was sufficient to meet the cooling requirements of ACC and MED in both hot and cold seasons. A potential savings of 2.5% of the power loss in a CCPP was realized on a hot summer day for this TES system, along with an estimated desalination capacity of 950-1,600 m^3/d for top brine temperatures between 100 °C and 70 °C in the MED. The main characteristics of non-solar desalination technologies are summarized in Table 9.

2-4. Pressure-retarded Osmosis and Reverse Electrodialysis

The salinity-gradient energy is a type of renewable and gas emission-free energy that is based on the release of free energy of mixing upon mixing of waters with different salt concentrations [152; 153]. The membrane-based desalination technologies can be used to generate power from salinity-gradient energy when operated in the reversed mode. Two types of membrane-based processes for energy conversion of salinity-gradient energy are pressure-retarded osmosis (PRO), and reverse electrodialysis (RED) [154]. The power generated by PRO and RED as renewable energy sources can be used to power the desalination systems. Among the desalination processes, RO process is most attractive for integrating with PRO and RED systems due to similarity of processes (membrane-base). In the RO-PRO and RO-RED systems the brine of the RO process can be used as PRO and RED processes influent without the need for additional pre-treatment.

Fig. 37 shows the diagram of RO-PRO system when low saline water is supplied as RO feed. As shown in Fig. 37, first the seawater and low salinity water is pretreated by a pretreatment unit. The pretreated seawater is sent to the PRO system as draw solution and low-saline water is passed through the RO membrane. The

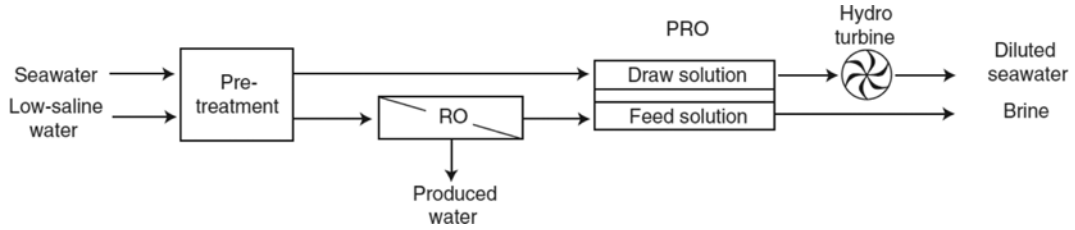

Fig. 37. Schematic of RO-PRO hybrid configuration [155].

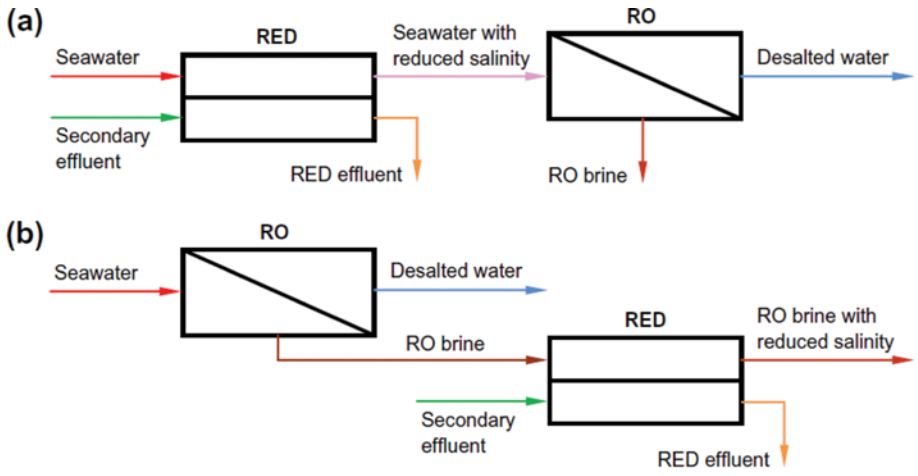

Fig. 38. Schematic diagram of the basic RO-RED hybrid processes [156].

brine of the RO system is used as the feed solution for PRO. The high salinity water flow draws the less concentrated water through the membrane due to its higher osmotic pressure, which leads to increase in volume of flow. The high volume flow is passed through a hydropower turbine to generate a portion of required RO electric power. Four possible configurations of hybrid RO-PRO process have been investigated by Kim et al. [155].

There are two basic configurations for RO-RED systems based on different assemblages of the RED and RO units. As shown in Fig. 38(a), in the first system (RED→RO mode) seawater as concentered salt solution and a secondary effluent as a diluted solution pass the RED unit to filed between the membranes. The salinity gradient results in a potential difference (e.g., 80 mV for seawater and river water) over each membrane, which causes the transport of ions through the membranes from the concentrated solution to the diluted solution. For a sodium chloride solution, sodium ions pass through the cation exchange membrane in the cathode direction, and chloride ions pass through the anion exchange membrane in the anode direction. The electrical current and the potential difference over the electrodes are used to generate electrical power by connecting an RO electric pump to the circuit. The seawater with reduced salinity is passed through the RO membrane to produce freshwater. In the second configuration (RO→RED mode) shown in Fig. 38(b), first seawater is passed through the RO membrane where the freshwater is produced and brine is used as the concentrated salt solution for RED unit [156].

In all RO-PRO and RO-RED configurations, the RO energy consumption and adverse environmental impact that seawater RO brine disposal can have on marine ecology are reduced compared to an optimized RO system with an energy recovery device [156,157].

SYSTEM ANALYSIS

Any analysis of solar thermal systems will be incomplete without including the thermodynamic and economic perspectives. The primary objective in the design and optimization of solar distillation processes is to maximize the available solar energy while restricting heat losses from the system to minimum thermodynamic and economic levels, which in turn obtains the maximum output (distilled water) in both quantity and quality (i.e., to maximize still productivity). Quantity and quality of energy transfer as well as the cost of components should be investigated throughout the distillation processes. Therefore, a thorough analysis of convection and radiation processes should be based on economic analysis and energy conservation principles, including the exergy balance of the process [158-160] and thermoeconomic analysis.

1. Exergy Analysis

In brief, exergy analysis is a method that implements the conservation of mass and conservation of energy principles together with the second law of thermodynamics for the analysis, design, optimization, and improvement of energy systems. Exergy analysis is used to complement rather than to substitute for energy analysis [23,161].

Based on the first and second laws of thermodynamics, the following exergy balance equation is obtained [162,163]:

$$\dot{E}x_Q + \sum_i \dot{E}x_i = \sum_e \dot{E}x_e + \dot{E}x_w + \dot{E}x_D \tag{75}$$

where subscripts e and i represent inlet and outlet specific exergy of the control volume, respectively, and Ex_D is exergy destruction. Other terms in this equation are as follows [Wonchala et al., 2014; Janghorban Esfahani and Yoo, 2013a]:

$$\dot{E}x_Q = \left(1 - \frac{T_0}{T_i}\right)\dot{Q}_i \tag{76}$$

$$\dot{E}x_w = \dot{W} \tag{77}$$

$$\dot{E}x = \dot{m}ex \tag{78}$$

where ex is the overall exergy of the stream calculated by Eq. (79)

$$e = (h - h^*) - T_0(s - s^*) + \sum_{i=1}^{n} x_i(\mu_i^* - \mu_i^0) \tag{79}$$

where e, h, T, s, x, and μ are specific exergy, specific enthalpy, temperature, specific entropy, mass fraction, and chemical potential, respectively. Subscript i represents the number of substances in the system. Superscript '0' refers to ambient pressure, temperature, and

concentration conditions, while superscript '*' refers to ambient pressure and temperature, and initial concentrations of the system conditions [4,164,165].

When calculating exergy, specific entropy, enthalpy, and chemical potential of the seawater at a specified temperature T, pressure P, and concentration x are estimated by correlations from ref. [166, 167]. The exergy efficiency of any process is a ratio of the exergy transfer rate associated with the output to the exergy transfer rate associated with the driving input [168]. Thus exergy or the second Law of efficiency is defined as follows:

$$\eta_{ex}=\frac{\text{Exergy output}}{\text{Exergy input}}=1-\frac{\text{Exergy destruction or irreversibilities}}{\text{Exergy input}} \quad (80)$$

Exergetic efficiencies are useful for identifying means for the utilization of energy resources that are thermodynamically effective. They can also be used to evaluate the effectiveness of engineering measures taken to improve the performance of a thermal system. This can be done by comparing efficiency values determined before and after modifications have been made to assess how much improvement has been achieved. The value of η_{ex} is generally less than unity even when η_e=1 [169]. In solar energy systems, η_{ex} is very low compared to the same value in other energy systems, as discussed in the next section. The thermal radiation from the sun is relatively rich in exergy [170], but the exergy efficiency of solar thermal collectors or systems is low. An extensive review of the problems of radiation exergy is provided by Bejan [158]. Some clarifications regarding the exergy of thermal radiation have been provided by Petela [159], who blamed the low efficiency of solar thermal devices on the impossibility of full absorption of the insolation. In this view, to obtain high quality energy at high temperatures, the absorbing surface also has to be at high temperature, which results in a major loss of energy by emission from the surface. This factor influences both energy and exergy efficiencies. Such a large exergy loss takes place during the absorption of solar radiation by the absorber surface at temperatures much lower than the temperature of the sun as a black body radiation source [171,172]. Another factor that makes exergy efficiency lower than energy efficiency in solar thermal devices is a significant degradation of energy quality. The relatively high temperature (approximately 6,000 K) of solar radiation is degraded to a relatively low temperature, e.g., to the temperature of heated water, which is not much greater than the atmospheric temperature, the temperature required for drying crops, solar cooking temperature, or the temperature required for photosynthesis [23]. The exergy of solar radiation can be calculated by Eq. (81).

$$Ex_{sun}=G_s\cdot A\cdot\psi \quad (81)$$

where G_s is the energy of solar radiation, A is the area of surface of the solar device on which the solar radiation is incident, and ψ is the Petela expression presented in Eq. (8), which presents the relative potential of maximum energy available from solar radiation energy [159,171,172].

$$\psi=1+\frac{1}{3}\left(\frac{T_0}{T_s}\right)^4-\frac{4}{3}\left(\frac{T_0}{T_s}\right) \quad (82)$$

where T_0 is ambient temperature and T_s is solar temperature.

Caliskan et al. [173] modeled and analyzed hybrid renewable energy-based hydrogen and electricity production and storage systems by utilizing energy, exergy and sustainability approaches. They considered several subsystems, including a hybrid geothermal energy-wind turbine-solar photovoltaic (PV) panel, inverter, electrolyzer, hydrogen storage system, proton exchange membrane fuel cells (PEMFC), and battery and loading systems. A case study based on a hybrid wind-solar renewable energy system was also conducted. The dead state temperatures were set to 0 °C, 10 °C, 20 °C and 30 °C, while the environmental temperature was 30 C. The maximum efficiencies of the wind turbine, solar PV panel, electrolyzer, and PEMFC are calculated as 26.15%, 9.06%, 53.55%, and 33.06% through energy analysis, and 71.70%, 9.74%, 53.60%, and 33.02% through exergy analysis, respectively. The overall exergy efficiency, ranging from 5.838% to 5.865%, is directly proportional to the dead state temperature and becomes higher than the corresponding energy efficiency of 3.44% for the entire system.

Banat and Jwaied [174] employed exergy analysis to evaluate the exergy efficiency of "compact" and "large" solar driven MD desalination units. The exergy efficiency of the compact and large units was calculated with reference to the exergy collected by the solar collector to be about 0.3% and 0.5%, but was 0.01% and 0.05%, respectively, when referenced to the exergy of solar irradiance. The exergy efficiency of the flat plate solar collectors in both units varied diurnally, and the maxima were 6.5% and 3% for the compact and large units, respectively. The greatest exergy destruction occurs within the membrane distillation module.

Al-Sulaiman et al. [175] used exergy modeling to assess the exergetic performance of a novel trigeneration system using parabolic trough solar collectors (PTSC) and an organic Rankine cycle (ORC). They considered four cases: electrical power, cooling-cogeneration, heating cogeneration, and trigeneration. In their proposed trigeneration system, a single-effect absorption chiller was utilized to provide the necessary cooling energy and a heat exchanger was utilized to provide the necessary heating energy. The trigeneration system was examined using three modes of operation: solar mode during the low-solar radiation times of day, solar and storage mode during the high solar radiation times of day, and storage mode during the night. Storage mode is operated using heat collected in a thermal storage tank other modes of operation. Exergy efficiencies and exergy destruction rates were examined according to ORC evaporator pinch point temperature, ORC pump inlet temperature, and turbine inlet pressure. The maximum electrical-exergy efficiency for the solar mode is 7%, for the solar and storage mode is 3.5%, and for the storage mode is 3%. Alternatively, when trigeneration was used, the exergy efficiency increased noticeably, with the maximum trigeneration-exergy efficiency for the solar mode 20%, for solar and storage mode 8%, and for storage mode 7%. Moreover, the main sources of exergy destruction are solar collectors and ORC evaporators. Therefore, careful selection and design of these two components are essential to reduce the destroyed exergy and, thus, increase the exergy efficiencies of the system.

2. Economic Analysis

Many factors affect the economics of desalination, such as intake water quality, plant capital cost, energy cost, labor and mainte-

Table 10. Cost analysis formulation for water distillation unit [176]

Equation	Description	No.
$CRF=i(1+i)^n/[(1+i)^{n-1}]$	CRF=capital recovery factor I=the interest per year (12%) N=the number of life years (10)	(83)
FAC=P(CRF)	FAC=fixed annual cost	(84)
$CFF=i/[(1+i)^{n-1}]$	SFF=Sinking fund factor	(85)
S=0.2P	P=is the present capital cost (700$)	(86)
AMC=0.15(FAC)	AMC=maintenance cost	(87)
ACC=CC? ower	CC=current cost=0.06 $/kW h ACC=The cost of power used in system	(88)
AC=FAC+AMC−ASV	AC=annual cost	(89)
CPL=AC/M	M=annual yield of solar still CPL=cost of distilled water per liter	(90)

Table 11. Parameters of equations presented in Table 10

Type of solar still	Ref.	P	CRF	FAC	S	SFF	ASV	AMC	AC	M	CPL
Single slope solar still	[199]	275	0.177	49	55	0.057	3.5	7.5	53	1511	0.035
Single slope solar still	[200]	190	0.177	34	38	0.057	2	5	37	585	0.063
Single slope solar still	[201]	250	0.177	44.2	50	0.057	3	6.6	47.8	343	0.14
Solar still with solar collector	[201]	1144	0.177	202.5	228.8	0.057	13	30.4	219.9	1203	0.18
Solar still with solar collector	[202]	480	0.177	96	85	0.057	5.5	15.3	93	806	0.115
Solar still with solar concentrator	[203]	300	0.177	53.1	60	0.057	3.4	8	57.7	990	0.058
Solar still with sun tracking	[204]	300	0.177	53.1	60	0.057	3.4	8	57.7	250	0.23
Solar still with wick and fin type		250	0.177	44.3	50	0.057	3	6.6	47.9	731	0.065

nance cost, concentrate disposal cost, and financing interest rate. Energy plays the largest role in all desalination systems, i.e., the energy costs of thermal distillation seawater plants is close to 60% of the overall costs. If heat is supplied from the waste heat from the turbine exhaust energy costs become much lower.

The payback ratio depends on the cost of distilled water production and its applicability. The cost of distilled water per liter (CPL) can be calculated by dividing the net annualized cost of the system (AC) by the annual yield of the solar still (M). Cost analysis equations for water distillation units are presented in Table 10 with the parameters presented in Table 11. Increases in air flow rate and temperature cause the average cost of water production to increase [176].

For MSF plants with production capacities between 23,000 and 528,000 m^3/day, the water production cost ranges between 0.52 and 1.75 US$/$m^3$. For MED plants with production capacities of more than 90,000 m^3/day, the cost ranges between 0.52 and 1.01 $/$m^3$ [87]. Increasing productivity may lead to higher annual costs for the fresh water. The best cases are single-slope and pyramid-shaped solar stills that can produce 1,533 L/m^2 annually at a cost of around 0.0135 $/L [177]. Solar radiation heats the water and air, causing evaporation of water to produce distillate and movement of air through a chimney to produce power. If the plant is operated for eight days, the cost of water production is 2.23 $/$m^3$ which is lower than the cost of water produced by any other systems [178].

The cost of water produced by desalination units coupled with renewable energy resources is strongly related to the cost of energy produced using renewable energy sources. Despite the free cost of renewable energy, the capital cost of renewable energy systems is very high, which in turn increases water costs. However, by developing economic renewable energy technologies, capital costs may be reduced and therefore water production costs also decrease. Table 10 presents the average water production cost, and Table 12

Table 12. Average water production cost of solar desalination

Process	Specific cost	Ref.
SChD	2.23 ($/$m^3$ per 8 h in a day)	[178]
Single slope solar still	13.5 $/L/year	[177]
Solar assisted MSF	7.9 $/$m^3$	[205]
Desalination with MED	2-3.2 $/$m^3$	[183]
Solar assisted MSF	9 $/$m^3$	[206]
Solar pond assisted MED	0.52-0.62 $/$m^3$	[86]
Single-slope ST	14 $/$m^3$	[177]
Multi-effect ST	39.456 $/$m^3$	[41]
HDH	3.3 $/ m^3	[207]
HDH	61.65 $/$m^3$	[208]
Solar still	12.5 $/$m^3$	[209]
MESS	50 $/$m^3$	[210]
Solar still	0.52-2.99	[178]
Solar MD	9-18 $/$m^3$	[70]
PV-RO	6.5-29 $/$m^3$	[58,69]
PV-ED	5.8-16 $/$m^3$	[198]

summarizes a cost analysis of solar still desalination processes.

2-1. Solar Thermal Desalination

2-1-1. Solar Still

The capital cost of solar stills is low and fossil fuel is not necessary to evaporate the water. However, due to the low productivity of these stills the water production costs remain high. The average daily production rate of such stills ranges from 4 to 6 L/m^2 [PRODES, 2010], and the water costs range between 0.52 [228] and 14 $/m^3 [177].

2-1-2. Solar Multi-effect Humidification

Low-temperature heat and electricity are required in MEH units. The sizes of existing MEH units range from 1 to 100 m^3/ day, and the average total energy consumption (both thermal and electrical) is about 31.1 kWhe/m^3. The water production costs of these units range from 2.6 to 6.5 US$/m^3 [179].

2-1-3. Solar Pond Desalination

The temperature of the storage zone of a solar pond may be higher than 90 °C. This energy can be used to provide heat in both MED and MSF desalination processes. The cost of the water from produced by SP/MED units ranges from 0.71 to 0.89 US$/m^3 [179,180].

2-1-4. MSF and MED

Solar-assisted MSF and MED processes have productivities of 6-60 and 6-13 L/m^2/day, which is greater than those of direct processes. The production cost of MSF is 2.5-7.6 $/m^3. These processes exhibit better function if they are integrated with solar ponds or solar collectors. The average water production cost of MD is close to 16 $/m^3 [13]. Note that the cost of water produced by these systems can be reduced by increasing plant capacity.

3. Thermo-economic Analysis

Thermo-economic analysis combines exergy analysis and economic principles to design and operate cost-effective systems. This is a broader perspective than that used in conventional energy and economic analyses. It is an exergy-based cost minimization tool for thermal systems. Thermo-economic analysis is sometimes referred to as exergoeconomic analysis. Using this method, the thermodynamic inefficiencies of the system (exergy destruction and exergy losses and costs associated with such inefficiencies) are evaluated. This approach is referred to as exergy costing, in which a cost is associated with each exergy stream. Understanding these costs is useful for improving the cost effectiveness of the system and for reducing the cost of the final product of the system [161].

Thermo-economic analysis represents a branch of engineering that combines exergy analysis and cost principles to provide system designers and operators with information that is not available through conventional energy analysis and economic evaluations [1]. The thermo-economic balance of any unit is calculated based on exergy and cost balances. In a conventional economic analysis, a cost balance is usually formulated for the overall system operating at steady state as follows [181]

$$\sum \dot{C}_{in,\,k} + \dot{Z}_k^{CI} + \dot{Z}_k^{OM} = \sum \dot{C}_{out,\,k} \tag{91}$$

where C_{in}, and C_{out} are cost rates associated with streams to/from the component and Z^{CI} and Z^{OM} are the related costs of capital investment, operation, and maintenance of the kth component obtained using the economic models described in section 1.2 [12].

In applications of the cost balance equation (Eq. (1)) there is usually more than one inlet-outlet stream for some of the components. Therefore, the number of unknown cost parameters is greater than the number of cost balance equations for the component. To solve this problem, auxiliary thermodynamic equations were developed according to the P and F rules [12,182]. Based on these rules, the product is defined as being equal to the sum of all of the exergy values that are taken into consideration at the outlet, plus all of the increases in exergy between the inlet and outlet that are in accordance with the purpose of the component. Similarly, fuel was defined as being equal to all of the exergy values that are taken into consideration at the inlet plus all of the decreases in exergy between the inlet and outlet, minus all of the exergy increases that are not in accordance with the purpose of the component [2].

Many investigations of thermal power plants, cogeneration, and other energy systems using thermo-economic analysis have been performed. Such analyses have proven very useful for optimizing entire systems or specific variables within a single component. Basic equations for the thermo-economic analysis of desalination systems are available elsewhere [6]. Thermo-economic analyses of desalination and other solar energy systems are rare.

Ranjan and Kaushik [23] investigated solar still systems in the context of energy, exergy, and thermo-economic analyses. They found that the energy efficiency and productivity of conventional solar stills is normally low, in the range of 20-46% and less than 6 L/m^2/day, respectively, even under optimized operating conditions. The exergetic efficiencies were estimated to be between 19% and 26% for a triple effect system, 17-20% for a double effect system, and less than 5% for a single effect system. Productivity is increased significantly by the use of integrated solar stills with better efficiency. The overall energy and exergy efficiency of integrated systems increases to 62% and 8.5%, respectively, using single effect solar stills. A literature review indicated that the cost of desalination through solar stills ranges from US$ 0.014 to 0.237/L and decreases further with increases in efficiency. Integrated solar desalination systems and technologies are better choices than conventional solar distillation systems for rural as well as urban areas with sufficient sunshine.

Sharaf et al. [1] thermodynamically evaluated solar energy with different configurations of multi-effect distillation process. They considered two different types of combined solar cycles with different configurations of multi effect distillation (MED) processes. In the first technique, solar energy is directly utilized from the solar collector field via an evaporator heat exchanger supplying the first effect of the MED process. This technique produces only potable water. In the second technique, the exhausted energy from an organic Rankine cycle (ORC) turbine is used in the first effect of the MED process to produce power electricity as well as desalted water. They studied two systems, one with a parabolic trough collector (PTC) with toluene organic oil and water working fluids. Therminol-VP1 heat transfer oil (HTO) was considered for indirect vapor generation across the solar field and evaporator heat exchanger. Comparisons were manipulated assuming 100 m^3/day of distillate product. The desalination-alone technique was considered more attractive than the combined desalination and power technique due to its higher gain ratio and the smaller solar field area needed. The parallel feed configuration is dominant against the forward feed with a feed heater configuration, while increas-

ing the number of effects to more than 12. Sharaf et al. [2012a] thermodynamically compared different types of solar desalination processes and showed that RO and multi effect distillation thermal vapor compression were superior, according to specific solar area, total water price, thermo-economic product cost, and the gain ratio. The systems were based on two scenarios: (1) different operating conditions due to each individual technology, and (2) uniform operating conditions.

Sharaf et al. [7] thermo-economically analyzed different solar power assisted techniques of MED-VC (multi effect distillation-vapor compression) processes. Two techniques for solar power cycles were considered to power MED-PF-TVC, MVC (multi effect distillation thermal and mechanical vapor compressions). In the first technique, solar thermal power is directly transmitted from the solar collector field via a boiler heat exchanger unit toward the steam ejector of the MED-PF-TVC process. In the second technique, the electrical power generated by the SORC (solar organic Rankine cycle) is used to power the vapor compressor of the MED-PF-MVC process. This comparison was implemented according to the operation of a PTC (parabolic trough collector) with toluene organic oil and water working fluids (second technique). Therminol-VP1 HTO (heat transfer oil) was considered across the solar field, and water was considered for the boiler heat exchanger (1st technique). The case study assumed 4,545 m^3/day of distillate product. Reducing the value of the compression ratio while increasing the evaporator numbers reduced specific power consumption, solar field area, and thermo-economic costs. The operation of a steam ejector instead of increasing the evaporator's numbers increased the gain ratio.

4. Environmental Analysis

The environmental impacts associated with desalination systems can be categorized as greenhouse gas emission, temperature and salinity of discharged brine, and discharge of chemicals used in the pretreatment units.

All desalination technologies are powered by energy derived from the combustion of fossil fuels, which contribute to CO, CO_2, NO, NO_2, and SO_2 as well as several other harmful emissions. The amount of CO_2 is estimated to be 25 kg/m^3 of produced water [143,180]. Table 13 shows greenhouse gas emissions due to water production by desalination systems with respect to world population and oil required over the past five decades [183]. As presented in Table 13, currently the desalination capacity required worldwide is greater than 1.42 million tons of oil/day, which releases 156 metric tons of CO_2/day [143,183].

According to the Kyoto Protocol, several countries have committed to reduce global per capita emissions to 0.2-0.7 ton C/cap/year from current levels of 0.3 in developing countries, 5.5 in the USA; and 2.5 in Western Europe [184]. The use of renewable energy resources is an excellent alternative to overcome harmful gas emissions. Raluy et al. [185] carried out a global environmental analysis to estimate the environmental loads of renewable energy-powered desalination systems and examined the integration of renewable energies such as wind, solar, and hydropower with various types of thermal desalination technologies such as

Table 13. World population, desalination capacity, oil required and GHG emissions over past five decades [143,183]

Year	World population (billions)	World desalination capacity (million m^3/day)	Oil required (million metric tons day)	GHG emissions (metric tons CO_2/day)
1960	3.1	0.12	0	0.36
1970	3.8	0.72	0.02	2.16
1980	4.5	4.4	0.12	13.2
1990	5.3	13	0.36	39
2000	6	23	0.63	69
2008	6.8	52	1.42	156

Table 14. Air emissions of different RE-MSF systems [185]

Case study	RE-MSF	Kg CO_2/m^3 produced water	g NO_x/m^3 produced water	g SO_x/m^3 produced water
1	MSF (ST-S-EM)	11.027	10.201	20.385
2	MSF (ST-SP-EM)	10.915	9.819	19.858
3	MSF (DWH-EM)	1.98	4.46	14.96
4	MSF (DWH-WE 150 kW)	0.369	0.826	6.173
5	MSF (DWH-WE 2 MW)	0.317	0.842	5.912
6	MSF (DWH-PE-S 100 kWp)	1.1	2.519	11.926
7	MSF (DWH-PE-SP 100 kWp)	0.683	1.165	8.841
8	MSF (DWH-PE-S 500 kWp)	0.825	2.232	20.260
9	MSF (DWH-PE-SP 500 kWp)	0.546	1.42	13.008
10	MSF (DWH-HPE)	0.282	0.654	5.98
11	MSF (DWH-NM)	0.28	0.64	5.86

ST: solar thermal; DWH: driven waste heat; WE: wind energy; PE: photovoltaic energy; HPE: hydro-power energy; EM: European model; S: Switzerland; SP: Spain

Table 15. Air emissions of different RE-MED systems [185]

Case study	RE-MSF	Kg CO_2/m^3 produced water	g NO_x/m^3 produced water	g SO_x/m^3 produced water
1	MED (ST-S-EM)	8.260	7.085	20.533
2	MED (ST-SP-EM)	8.164	6.803	20.107
3	MED (DWH-EM)	1.19	2.53	19.59
4	MED (DWH-WE 150 kW)	0.309	0.688	11.811
5	MED (DWH-WE 2 MW)	0.283	0.696	11.682
6	MED (DWH-PE-S 100 kWp)	0.675	1.536	14.699
7	MED (DWH-PE-SP 100 kWp)	0.363	0.902	14.992
8	MED (DWH-PE-S 500 kWp)	0.536	1.393	18.859
9	MED (DWH-PE-SP 500 kWp)	0.397	0.986	15.232
10	MED (DWH-HPE)	0.265	0.604	11.62
11	MED (DWH-NM)	0.27	0.6	11.66

ST: solar thermal; DWH: driven waste heat; WE: wind energy; PE: photovoltaic energy; HPE: hydro-power energy; EM: European model; S: Switzerland; SP: Spain

MSF, and MED. Tables 14 and 15 present their evaluations of CO_2, NO_x, and SO_x for MSF and MED, respectively, integrated with renewable energies. In case studies 1 and 2 the required thermal energy is generated by solar flat plate collectors, whereas in case studies 3-11 the thermal energy is provided by other industrial processes, and the thermal energy is low temperature waste heat. Electricity is provided by different sources such as in the European model (43.3% thermal, 40.3% nuclear and 16.4% hydroelectric) [186], Norwegian model (0.5% thermal, 0.3% nuclear and 99.2% hydroelectric) [186], photovoltaic, wind energy, and hydropower. The results obtained by Raluy et al. [185] show that increases of 92.5% and 20% in the wind plant and photovoltaic production capacity cause decreases of 20% and 19% in all air emissions, respectively. A 50% increase in solar radiation results in decreases of 38% and 36% in air emissions. For systems that are fully integrated with other industrial processes the use of renewable energies decreases emissions by 70%. CO_2 and SO_X have the highest and lowest reduction effects, with averages of 72% and 44%, respectively, among air emissions. Raluy et al. [185] obtained similar results to those for RE-MSF and RE-MED presented in Tables 14 and 15 respectively.

Seawater desalination plants are located at coastal sites which are a sensitive environmental habitat [187]. High salinity brine is a byproduct of desalination with undesirable environmental effects. It is generally produced as a liquid with very high salt concentrations. The salinity of the discharge from RO plants is about 100% higher than the salinity of seawater at ambient temperatures, whereas the salinity of the discharge from distillation (MSF or MED) plants is about 15% higher than that of seawater and is released at a temperature of 50 to 100 °C higher than ambient. Multi-stage flash (MSF) and other forms of thermal distillation tend to have the greatest impact on intake water temperature, and can release brines 10-15 °C warmer than oceanic waters [188,189]. Therefore, distillation plants have greater negative impacts on, and represent greater risks to, marine and aquatic life, because higher temperatures reduce the overall concentrations of dissolved oxygen in the receiving waters, therefore threatening life that cannot exist at low oxygen levels. The distribution and extent of thermal impacts is influenced by the location of the plant discharge, with brine discharges to enclosed water bodies more likely to result in measurable thermal effects than discharges to well-flushed environments [190]. The RO process requires more intensive pretreatment than do distillation processes. Among desalination processes such pretreatment is usually in the form of chemical additives that have direct and indirect impacts on aquatic marine life. However, the levels of these chemicals are generally relatively low [191].

Large volumes of seawater are extracted and hypersaline brine is discharged into the marine environment by desalination plants. The urgent need for water in many regions has meant that marine environmental issues associated with desalination have been considered secondary concerns [192]. Table 16 summarizes the extent and intensity of brine plumes in receiving water surrounding desalination plant discharge outlet [190].

4-1. Discharge Options

Brine disposal is a major environmental problem of seawater desalination plants. If a feasible and efficient alternative to ocean disposal could be found, the entire problem of marine pollution would be solved. Conventional disposal methods of desalination plants comprise:

- Disposal to surface water
- Disposal to sewer
- Deep well injection
- Evaporation ponds
- Land application, e.g. irrigation

The most widely used disposal methods in the USA are surface water discharge (45%), sewer discharge (27%) and deep well injection (13%) [187].

4-2. Discharge Design

The concentration of a pollutant discharge depends on the initial discharge concentration, the concentration in the ocean and the level of dilution [193]. The pollutant concentration after ith dilution is defined as:

$$d_i = \frac{y + i*x}{i+1} \quad (92)$$

Where

Table 16. Extent and intensity of brine plumes in receiving waters surrounding desalination plant discharge outlets

Reference	Capacity (ML/d)	Discharge (ML/d)	Salinity of brine (ppt)	Location	Habitat	Plume extension and intensity
[211]	92.4	NR	37.3	Muscat, Oman	Soft sediments	Returned to background levels within approximately 100 m of outlet
[211]	191	NR	40.11	Muscat, Oman	Soft sediments	Appeared to return to background levels 980 m from outlet
[212]	106	288	51	Sitra Island, Bahrain	Soft sediments	Salinity of receiving water reach 51 ppt, relative to reference areas of 45 ppt, plume extended at least 160 m from discharge. Temperature also affected, discharged at 10-15 °C above ambient, receiving water up to 7 °C above ambient
[213]	9.1	22	40-55	Florida, USA	Artificial hard substrata and soft sediments	0.5 ppt above background levels within 10-20 m of outlet. Nevertheless, slight elevation was maintained for 600 m within the harbour basin
[214]	25	17	75.2	Canary Islands, Spain	Sub-tidal rocky reef	2 ppt above background on the seabed and 1 ppt on the surface within the 20 m of the outlet; similar to background levels at 100 m.
[215]	NR	NR	NR	Dhkelia, Cyprus	NR	Above background 100-200 m from outlet, occasionally as high as 60 ppt.
[216]	50	75	68	Alicante, Spain	Seagrass and soft sediments	0.5 ppt above ambient for up to 4 km from outlet along the seafloor
[217]	28	NR	44	Javea, Spain	Seagrass and soft sediments	Slightly above background up to 300 m from the outlet
[218]	60	33	60[a]	Blanes, Spain	Seagrass and soft sediments	At background levels within 10 m of outlet. No apparent measurement or analysis of salinity
[219]	50	65	68	Alicante, Spain	Soft sediments	2.6 ppt above ambient within 300 m[b] of outlet; 1 ppt within 600 m[b]; similar to background at 1,300 m[b]
[192]	274	600	42	Ashkelon, Israel	NR	Approximately 2 ppt above ambient within 400 m of outlet, <1 ppt above ambient within 4,000 m of the outlet
[220]	25	NR	75	Canary Islands, Spain	Soft sediments	75 ppt effluent diluted to 38 ppt within 20 m of outlet, no details given as to background salinity
[221]	NR	2	60	Formentera, Balearic Islands, Spain	Seagrass and soft sediments	5.5 ppt above background 10 m from outlet; 2.5 ppt at 20 m; 1 ppt at 30 m; not measured any further than this

NR=not reported
[a]- g/L
[b]Inferred from figure, estimate only

y=discharge concentration
x=receiving water concentration
i=dilution number
d_i=pollutant concentration after ith dilution

A simple way to provide good effluent dilution and to minimize the environmental effects is to discharge into a highly energetic sea location where no sensitive ecosystems are in reach. The concentrate not only includes brine but also includes chemicals

Table 17. Chemicals used in pretreatment and post-treatment of desalination plants [194]

Pretreatment		Post-treatment	
Chemical	Purpose	Chemical	Purpose
NaOCl	Prevention of biological growth	Enzymes	Breaking down of bacteria
$FeCl_3$/$AlCl_3$	Flocculation and removal of suspended matter from water	Detergents, surfactants and caustics	Resuspension of particulate matter and dissolving of organic material and silica
H_2SO_4/HCl	Adjustment of pH	Biocides	Killing bacteria
$NaHSO_3$	Neutralization of chlorine in feedwater	Chelators	Removing scale
Scale inhibitors	Prevention of scale formation	Acids	Dissolving inorganics

used from pretreatment and post-treatment, which are added to the pipe of the concentrate before its disposal and add to the negative impact of the concentrate. These chemicals are summarized in Table 17 with their purposes [194].

CONCLUSION

Renewable energy-powered thermal desalination systems were comprehensively investigated and compared in this review. Among all of the processes described, solar stills are the most economically suitable but occupy large areas. The water produced by a solar still is of high quality but productivity is very low, between 4 and 6 L/m^2/day; therefore, the water production costs are high at 0.5 to 14 $/$m^3$. Solar based humidification-dehumidification systems are more flexible than other direct processes and require large numbers of stages for efficient operation, which increases system costs such that these systems are suitable primarily for low capacity decentralized operations. Solar chimneys can produce not only power and water but also byproducts such as salt. Solar chimneys require large areas to operate and are therefore feasible only in wastelands or coastal areas. They have the lowest production costs, but such structures are very heavy, so the capital costs are the highest among technologies. MSF, MED and VC systems are mature technologies, but there are few studies of long-term operating issues when coupled with solar systems. Absorption desalination systems are very suitable when refrigeration and fresh water are required simultaneously, while natural vacuum solar desalination systems are superior in remote mountainous areas.

Furthermore, energy and economic analyses indicate that the increasing efficiency of renewable energy powered-thermal desalination systems enabled by the modification of system design contributes to higher system costs and consequently higher freshwater production costs. These freshwater production costs can be decreased by ensuring the maximum utilization of renewable energy sources and minimum component sizes, exergy destruction, and environmental emissions. We believe that renewable powered-thermal desalination systems are undoubtedly valuable around the world where freshwater and fossil fuel resources are being reduced. However, the freshwater production costs by these systems are high compared to the conventional systems. Therefore, studies to reduce the cost and environmental impact of renewable powered-thermal desalination systems are essentially as follows:

- Exergo-environ-economic analysis and optimization to achieve the most efficient and reliable renewable powered desalination system for various capacities
- Process hybridization to improve the economics and energy requirements
- Utilization of salinity-gradient energy to produce energy requirement of thermal desalination systems such as membrane distillation using pressure-retarded osmosis and reverse electrodialysis units

ACKNOWLEDGEMENTS

This work was supported by the National Research Foundation of Korea (NRF) grant funded by the Korean government (MSIP) (No. 2015R1A2A2A11001120).

REFERENCES

1. M. A. Sharaf, A. S. Nafey, and L. Garcia-Rodriguez, *Desalination*, **272**, 135 (2011).
2. M. A. Eltawil, Zh. Zhengming and L. Yuan, *Ren. Sustain. Energy Review*, **13**, 2245 (2009).
3. I. Janghorban Esfahani and C. K. Yoo, *Energy*, **59**, 340 (2013).
4. I. Janghorban Esfahani, A. Ataei, K. V. Shetty, T. S. Oh, J. H. Park and C. K. Yoo, *Desalination*, **292**, 87 (2012).
5. N. Gaffour, J. Bundschuh, H. Mahmoudi and M. F. A. Goosen, *Desalination*, **356**, 94 (2015).
6. N. T. M. Gaffour and G. L. A. Missimer, *Desalination*, **309**, 197 (2013).
7. M. A. Sharaf, *J. Sol. Energy Eng.*, **134** (2012).
8. M. Goosen, H. Mahmoudi and N. Ghaffour, *Crit. Rev. Environ. Sci. Technol.*, **44**, 929 (2014).
9. M. T. Ali, H. E. S. Fath and P. R. Armstrong, *Renew. Sustain. Energy Rev.*, **15**, 4187 (2011).
10. H. A. Isam, *Desalination*, **239**, 207 (2009).
11. J. Wang, Y. Dai and L. Gao, *Appl. Energy*, **86**, 941 (2009).
12. I. Janghorban Esfahani and C. K. Yoo, *Energy*, **75**, 327 (2014).
13. H. M. Qiblawey and F. Banat, *Desalination*, **220**, 633 (2008).
14. L. Garzia-Rodriguez and C. Gomez-Camacho, *Desalination*, **136**, 213 (2000).
15. L. Garzia-Rodriguez, *Desalination*, **143**, 103 (2002).
16. M. Naim, A. Mervat and A. El-Kawi, *Desalination*, **153**, 55 (2003).
17. G. M. Mink Aboabbous and E. Karmazsin, *Sol. Energy*, **62**, 309 (1998).
18. R. Gugulothua, N. S. Somanchia, S. Rama Devi and H. B. Banoth, *Aquatic Procedia*, **4**, 1483 (2015).

19. E. S. H. Fath, *Desalination*, **116**, 45 (1998).
20. M. Malik, G. Tiwari, A. Kumar and M. Sodha, Pergamon Press, New York (1982).
21. O. Haddad, M. Al-Nimer and A. Maqableh, *Renew. Energy*, **21**, 459 (2000).
22. N. Setoodeh, R. Rahimi and A. Ameri, *Desalination*, **268**, 103 (2011).
23. K. R. Ranjan and S. C. Kaushik, *Renew. Sustain. Energy Rev.*, **27**, 709 (2013).
24. M. S. Sodha, A. Kumar, G. N. Tiwari and R. C. Tyagi, *Sol. Energy*, **26**, 127 (1981).
25. A. A. Al-Karaghouli and A. N. Minasian, *Renew. Energy*, **6**, 77 (1995).
26. F. Graeter, M. Duerrbeck and J. Rheinlaender, *Desalination*, **138**, 111 (2001).
27. A. El-Nashar and M. Samad, *Renew. Energy*, **14**, 263 (1998).
28. M. S. Sodha, J. K. Nayak, G. N. Tiwari and A. Kumar, *Energy Convers. Manage.*, **20**, 23 (1980).
29. M. Chaibi, Ph.D, Swedish University of Agricultural Sciences, Alnarp (2003).
30. M. T. Chaibi and T. Jilar, *Sol. Energy*, **76**, 545 (2004).
31. T. Arunkumar, D. Denkenberger, A. Ahsan and R. Jayaprakash, *Desalination*, **314**, 189 (2013).
32. K. Voropoulos, E. Mathioulakis and V. Belessiotis, *Desalination*, **164**, 189 (2004).
33. H. Fath and A. Ghazy, *Desalination*, **142**, 119 (2002).
34. Y. Assouad and Z. Lavan, *Sol. Energy Eng.*, **110**, 14 (1988).
35. S. Parekh, M. Farid, J. Selman and S. Al-Hallaj, *Desalination*, **160**, 167 (2004).
36. H. Müller-Holst, M. Engelhardt and W. Scholkopf, *Desalination*, **122**, 255 (1999).
37. H. Müller-Holst, M. Engelhardt, M. Herve and W. Scholkopf, *Renew. Energy*, **14**, 311 (1998).
38. E. Chafik, *Desalination*, **156**, 333 (2003).
39. H. Shaobo, Y. Shengquan and Zh. Hefei, *Desalination*, **183**, 143 (2005).
40. H. Shaobo, *Desalination*, **222**, 572 (2008).
41. S. Al-Hallaj, S. Parekh, M. M. Farid and J. R. Selmana, *Desalination*, **195**, 169 (2006).
42. G. Al-Enezi, H. Ettouney and N. Fawzy, *Energy Convers. Manage.*, **47**, 470 (2006).
43. Zh. Khalifa, *Renew. Sustain. Energy Review.*, **24**, 406 (2013).
44. M. T. Chaibi, *American J. Energy Res.*, **1**, 25 (2013).
45. C. Charcosset, *Desalination*, **245**, 214 (2009).
46. H. Sharon and K. S. Reddy, *Renew. Sustain. Energy Rev.*, **41**, 1080 (2015).
47. R. Sangi, *Renew. Sustain. Energy Rev.*, **24**, 704 (2012).
48. Z. Lu, Y. Zheng, Z. Li and Y. Shad, *Desalination*, **13**, 207 (2011).
49. F. Cao, H. Li, Y. Zhang and L. Zhao, *Sci. World*, 1 (2013).
50. H. F. Zheng, K. Y. He and Z. Q. Chen, Beijing Institute of Technology Press, Beijing (1991).
51. S. A. El-Agouz, *Energy*, **35**, 5108 (2010).
52. A. N. Minasian and A. A. Al-Karaghouli, *Energy Convers. Manage.*, **36**, 213 (1995).
53. S. L. Sirivinas, I. Janghorban Esfahani, P. Garikiparthy and C. K. Yoo, *Korean J. Chem. Eng.*, **32**, 1486 (2015).
54. J. H. Song, K. H. Yeon, J. Cho and S. H. Moon, *Korean J. Chem. Eng.*, **22**, 108 (2005).
55. K. He, H. J. Hwang and I. S. Moon, *Korean J. Chem. Eng.*, **28**, 770 (2011).
56. M. S. El-Bourawi, Z. Ding, R. Ma and M. Khayet, *J. Membr. Sci.*, **285**, 4 (2006).
57. M. Khayet, *Adv. Colloid Interface Sci.*, **164**, 56 (2011).
58. A. Alkhudhiri, N. Darwish and N. Hilal, *Desalination*, **287**, 2 (2012).
59. N. Palanisami, K. He and I. S. Moon, *Korean J. Chem. Eng.*, **31**, 155 (2014).
60. S. Kalogirou, *Progr. Energy Combust. Sci.*, **31**, 242 (2005).
61. P. Hogan, A. Sudjito, G. Fane and G. Morrison, *Desalination*, **81**, 81 (1991).
62. K. Thomas, *Renew. Energy Powered Desalination*, 1 (1997), (NREL/TP-440-22083, UC Category: 1210 DE 97000240).
63. F. Banat, N. Jwaied, M. Rommel, J. Koschikowski and M. Wieghaus, *Desalination*, **217**, 17 (2007).
64. X. Wang, L. Zhang, H. Yang and H. Chen, *Desalination*, **247**, 403 (2009).
65. F. Banat, R. Jumah and M. Garaibeh, *Renew. Energy*, **25**, 293 (2002).
66. A. Kullab and A. R. Martin, *Proceedings of the Sol. World Congress*, **27**, 32 (2005).
67. F. Banat and N. Jwaied, *Desalination*, **220**, 566 (2008).
68. L. Garcıa-Rodrıguez, *Sol. Energy*, **75**, 381 (2003).
69. M. Thomson and D. Infield, *Desalination*, **153**, 1 (2002).
70. M. R. Qtaishat and F. Banat, *Desalination*, **308**, 186 (2013).
71. J. K. Kim, D. P. Ju, *Korean J. Chem. Eng.*, **20**, 522 (2003).
72. D. Mourad, O. Ghazi and B. Noureddine, *Korean J. Chem. Eng.*, **26**, 1706 (2009).
73. R. K. Suri, A. M. R. Al-Marafie, A. A. Al-Homoud and G. P. Maheshwari, *Desalination*, **71**, 165 (1989).
74. D. Singh and S. K. Sharma, *Desalination*, **73**, 191 (1989).
75. R. Kriesi, *Desalination*, **39**, 109 (1981).
76. T. Szacsvay, P. Hofer-Noser and M. Posnansky, *Desalination*, **122**, 185 (1999).
77. S. M. A. Moustafa, D. I. Jarrar and H. I. El-Mansy, *Sol. Energy*, **35**, 333 (1985).
78. A. Hanafi, *Desalination*, **82**, 175 (1991).
79. M. J. Safi, *Renew. Energy*, **14**, 339 (1998).
80. H. Lu, J. C. Walton and A. H. P. Swift, *Desalination*, **136**, 13 (2001).
81. G. Micale, L. Rizzuti and A. Cipollina, *Springer Link* (2009).
82. K. Tahri, *Desalination*, **135**, 43 (2001).
83. M. J. Safi and A. Korchani, *Desalination*, **125**, 223 (1999).
84. D. W. J. Hayes and J. A. L. Kipps, *Desalination*, **88**, 301 (1992).
85. H. Lu, A. H. P. Swift, J. Hein and J. C. Walton, *Sol. Energy Eng.*, **126**, 759 (2004).
86. H. Lu, J. C. Walton and H. Hein, Desalination research and development program report no. 80, Cooperative Agreement No. 98-FC-81-0047 (2002).
87. Ch. Li, Y. Goswami and E. Stefanakos, *Renew. Sustain. Energy Rev.*, **19**, 136 (2013).
88. F. Trieb and H. Muller-Steinhagen, *Desalination*, **220**, 165 (2008).
89. S. Kalogirou, *Appl. Energy*, **76**, 337 (2003).
90. I. L. García, J. L. Alvarez and D. Blanco, *Sol. Energy*, **85**, 2443 (2011).

91. H. Shaobo, Z. Zhang, Z. Huang and A. Xie, *Desalination*, **220**, 524 (2008).
92. J. Jiang, H. Tian, M. Cui and L. Liu, *Renew. Energy*, **34**, 2798 (2009).
93. S. Kalogirou, *Energy*, **22**, 69 (1997).
94. T. Mezherand, H. Fath, Z. Abbas and A. Khaled, *Desalination*, **266**, 263 (2011).
95. P. T. Tsilingiris, *Desalination*, **103**, 249 (1995).
96. D. C. Alarcon-Padilla, L. Garcia-Rodriguez, *Desalination*, **212**, 294 (2007).
97. P. Palenzuela, G. Zaragoza, D. C. Alarcon-Padilla and J. Blanco, *Appl. Therm. Eng.*, **60**, 1514 (2011).
98. Ch. Li, Graduate Theses and Dissertations (2012).
99. D. Zhao, J. Xue, S. Li and H. Sun and Q. D. Zhang, *Desalination*, **273**, 292 (2011).
100. H. J. Joo and H. Y. Kwak, *Appl. Therm. Eng.*, **61**, 491 (2013).
101. H. Raach and J. Mitrovic, *Desalination*, **204**, 416 (2007).
102. G. Kronenberg, *Desalination*, **108**, 287 (1997).
103. V. V. Slesarenko, *Desalination*, **139**, 405 (2001).
104. D. C. Alarcón-Padilla, L. García-Rodríguez and J. Blanco-Gálvez, *Desalination*, **250**, 500 (2010).
105. A. Ophir and F. Lokiec, *Desalination*, **98**, 182 (2005).
106. C. Sommarva, *Desalination*, **222**, 592 (2008).
107. M. A. Darwish and A. Alsairafi, *Desalination*, **170**, 223 (2004).
108. O. Al Hawaj and M. A. Darwish, *Desalination*, **99**, 119 (1994).
109. M. A. Garman and M. A. Muntasser, *Desalination*, **222**, 689 (2008).
110. A. M. El-Nashar, *Desalination*, **93**, 597 (1993).
111. A. M. El-Nashar, *Desalination*, **130**, 235 (2000).
112. A. M. El-Nashar, *Desalination*, **130**, 217 (2000).
113. A. M. El-Nashar, *Desalination*, **239**, 66 (2009).
114. A. M. El-Nashar, *Desalination*, **134**, 173 (2001).
115. S. Kalogirou, *Renew. Energy*, **12**, 351 (1997).
116. E. Zarza, J. Ajona, J. León, A. Gregorzewski and K. Genthner, *Sol. Energy Mater.*, **24**, 608 (1991).
117. N. H. Aly and A. K. El-Figi, *Desalination*, **158**, 143 (2003).
118. F. Al-Juwayhel, H. El-Dessouky and H. Ettouney, *Desalination*, **114**, 253 (1997).
119. A. M. Helal and S. A. Al-Malek, *Desalination*, **197**, 273 (2006).
120. D. Zejli, A. Ouammi, R. Sacile, H. Dagdougui and A. Elmidaoui, *Appl. Energy*, **88**, 4042 (2011).
121. M. A. Sharaf, A. S. Nafey and L. Garcia-Rodriguez, *Energy*, **36**, 2753 (2011).
122. A. O. B. Amer, *Desalination*, **249**, 1315 (2009).
123. R. M. M. Kouhikamali, *Desalination*, **280**, 134 (2011).
124. R. Bahar, M. N. A. Hawlader and L. S. Woei, *Desalination*, **166**, 123 (2004).
125. D. Zejli, R. Benchrifa, A. Bennouna and O. K. Bouhelal, *Desalination*, **168**, 127 (2004).
126. S. C. Maroo and D. Y. Goswami, *Desalination*, **249**, 635 (2009).
127. S. Al-Kharabsheh and D. Y. Goswami, *Sol. Energy Eng.*, **126**, 774 (2004).
128. S. Al-Kharabsheh and D. Y. Goswami, *Sol. Energy*, **75**, 395 (2003).
129. M. Abutayeh and D. Y. Goswami, *AIChE J.*, **56**, 1196 (2009).
130. V. G. Gude and N. Nirmalakhandan, *Desalination*, **244**, 239 (2009).
131. T. Ayhan and H. Al Madani, *Renew. Energy*, **35**, 506 (2010).
132. V. G. Gude and N. Nirmalakhandan, *Energy Convers. Manage.*, **51**, 2245 (2010).
133. S. Al-Karabsheh and D. Y. Goswami, *Desalination*, **156**, 323 (2003).
134. V. G. Gude, N. Nirmalakandan, S. Deng and A. Maganti, *Appl. Energy*, **91**, 446 (2012).
135. V. G. Gude and N. Nirmalakandan, *Energy. Convers. Manage.*, **49**, 3326 (2008).
136. V. G. Gude, N. Nirmalakandan, S. Deng and A. Maganti, *Energy Convers. Manage.*, **56**, 192 (2012).
137. J. W. Wu, M. J. Biggs and E. J. Hu, *Chem. Eng. Res. Des.*, **88**, 1541 (2010).
138. J. W. Wu, M. J. Biggs and E. J. Hu, *Appl. Energy*, **90**, 316 (2012).
139. J. W. Wu, M. J. Biggs, P. Pendelton, A. Badalyan and E. J. Hu, *Appl. Energy*, **98**, 190 (2012).
140. K. Thu, K. C. Ng, B. B. Saha, A. Chakraborty and S. Koyama, *Heat Mass Transf.*, **52**, 1811 (2009).
141. K. C. Ng, K. Thu, B. B. Saha and A. Chakraborty, *Int. J. Refrig.*, **35**, 685 (2012).
142. K. Thu, B. B. Saha, A. Chakraborty, W. G. Chun and K. C. Ng, *Heat Mass Transf.*, **54**, 43 (2011).
143. V. G. Gude, N. Nirmalakhandan and S. Deng, *Renew. Sustain. Energy Rev.*, **14**, 2641 (2010).
144. K. Bourouni, R. Martin and L. Tardist, *Desalination*, **122**, 301 (1999).
145. K. Bourouni and J. C. Deronzierb, *Desalination*, **125**, 147 (1999).
146. Karytsas, EURORED Network. Santorini, Greece: *CRES*, 128 (1996).
147. J. A. Carta, J. Gonzalez and V. Subiela, *Sol. Energy*, **75**, 153 (2003).
148. U. Plantikow, *World Wind Energy Conference* (2003).
149. C. R. Henderson, J. G. McGowan and J. F. Manwell, *Global WINDPOWER Conference and Exhibition* (2004).
150. V. G. Gude and N. Nirmalakhandan, *ASCE J. Energy Eng.*, **134**, 95 (2008).
151. V. Gadhamshetty, V. G. Gude and N. Nirmalakhandan, *Energy*, **66**, 938 (2014).
152. F. Helfer, C. Lemckert and Y. G. Anissimov, *J. Membr. Sci.*, **453**, 337 (2014).
153. S. S. Hong, W. Ryoo, M. S. Chun and G. Y. Chung, *Korean J. Chem. Eng.*, **32**, 1249 (2015).
154. J. W. Post, J. Veerman, V. M. Hamelers Hubertus, G. J. W. Euverink, S. J. Metz, K. Nymeijer and C. J. N. Buisman, *J. Membr. Sci.*, **288**, 218 (2007).
155. J. Kim, M. Park, S. A. Snyder and J. H. Kim, *Desalination*, **322**, 121 (2013).
156. W. Li, W. B. Krantz, E. R. Cornelissen, J. W. Post, A. R. D. Verliefde and C. Y. Tang, *Appl. Energy*, **104**, 592 (2013).
157. J. Prante, J. Ruskowitz, A. E. Chilress and A. Achilli, *Appl. Energy*, **120**, 104 (2014).
158. A. Bejan, Hoboken, Wiley, New Jersey (2006).
159. R. Petela, The McGraw-Hill Companies, Inc. (2010).
160. I. Dincer and M. A. Rosen, Elsevier (2007).
161. A. Bejan, G. Tsatsaronis and M. Moran, Wiley, New York (1996).
162. Z. G. Sun, *Energy*, **6**, 431 (2008).
163. I. Janghorban Esfahani, Y. T. Kang and C. K. Yoo, *Energy*, **75**, 312 (2014).
164. I. Janghorban Esfahani and C. K. Yoo, *Energy*, **59**, 340 (2013).
165. I. Janghorban Esfahani, S. C. Lee and C. K. Yoo, *Desalination*, **359**, 92 (2015).

166. M. H. Sharqawy, J. H. V. Lienhard and S. M. Zubair, *Int. J. Therm. Sci.*, **50**, 187 (2011).
167. Y. Kaita, *Int. J. Refrig.*, **24**, 374 (2001).
168. T. J. Kotas, *The exergy method of thermal power plant analysis*, Butter worths (1985).
169. M. J. Moran and H. N. Shapiro, *Fundamentals of engineering thermodynamics*, Wiley, New Delhi, India (2010).
170. R. Petela, *Heat Trans. ASME*, **2**, 187 (1964).
171. R. Petela, *Sol. Energy*, **74**, 469 (2003).
172. R. Petela, *Int. J. Exergy*, **7**, 89 (2010).
173. H. Caliskan, I. Dincer and A. Hepbasli, *App. Therm. Eng.*, **61**, 784 (2013).
174. F. Banat and N. Jwaied, *Desalination*, **230**, 27 (2008).
175. F. A. Al-Sulaiman, I. Dincer and F. Hamdullahpur, *Sol. Energy*, **85**, 2228 (2011).
176. S. A. El-Agouz, *Chem. Eng.*, **165**, 413 (2010).
177. A. E. Kabeel, A. M. Hamed and S. A. El-Agouz, *Energy,* **35**, 2901 (2010).
178. M. F. A. Goosen, S. S. Sablani, W. H. Shayya, C. Paton and H. Al-Hanai, *Desalination*, **129**, 63 (2000).
179. PRODES, Roadmap for the development of desalination powered by renewable energy, *Intelligent Energy*, Europe (2010).
180. A. A. Al-Karaghouli and L. L. Kazmerski, *Desalination Trend. Techno.*, National Renewable Energy Laboratory Golden, Colorado, **80401**, INTECH Publisher (2011).
181. A. Bejan, G. Tsatsaronis and M. Moran, *Handbook of Thermal Design and Optimization*, Wiley, New York (1996).
182. I. Janghorban Esfahani and C. K. Yoo, *Desalination*, **332**, 18 (2014).
183. G. Fiorenza, V. K. Sharma and G. Braccio, *Energy. Convers. Manage.*, **44**, 2217 (2003).
184. A. Lamei, P. Van Der Zaag and E. Von Munch, *Energy Policy*, **36**, 1748 (2008).
185. R. G. Raluy, L. Serra and J. Uche, *Desalination*, **183**, 81 (2005).
186. M. Lenzen and J. Munksgaard, *Renew. Energy*, **26**, 339 (2002).
187. W. I. Frank Munk, Dimploma Thesis, university of Karlsruhe (2008).
188. T. Hoepner, *Desalination*, **124**, 1 (1999).
189. S. Lattemann and T. Höpner, *Desalination*, **220**, 1 (2008).
190. D. A. Roberts, *Water Res.*, **44**, 5117 (2010).
191. M. Dawoud and M. Al Mulla, *Environ. Sustain.*, **1**, 22 (2012).
192. I. Safrai and A. Zask, *Desalination*, **220**, 72 (2008).
193. M. Mickley, *Membrane concentrate disposal*, Practices and regulation, 2nd Ed. (2004).
194. T. Younos, *Contemporary Water Research & Education*, **132**, 11 (2005).
195. M. K. Gupta and S. C. Kaushik, *Renew. Energy*, **35**, 1228 (2010).
196. R. Jain, *Clean Technol. Environ. Policy*, **14**, 1 (2012).
197. R. V. Dunkle, *The international heat transfer conference*, ASME, USA, **5**, 895 (1961).
198. A. Al-Karaghouli, L. Lawrence and L. Kazmerski, *Renew. Sustain. Energy Rev.*, **24**, 343 (2013).
199. H. E. S. Fath, M. El-Samanoudy, K. Fahmy and A. Hassabou, *Desalination*, **159**, 69 (2003).
200. M. A. Samee, U. K. Mirza, T. Majeed and N. Ahmad, *Renew. Sustain. Energy Rev.*, **11**, 543 (2007).
201. S. Kumar and G. N. Tiwari, *Appl. Energy*, **86**, 1995 (2009).
202. O. O. Badran and H. A. Al-Tahaineh, *Desalination*, **183**, 137 (2005).
203. Z. S. Abdel-Rehim and A. Lasheen, *Desalination*, **217**, 52 (2007).
204. S. Abdallah and O. O. Badran, *Desalination*, **220**, 669 (2008).
205. S. Farzad and A. Behzadmehr, *Desalination*, **278**, 70 (2011).
206. J. Joseph, R. Saravanan and S. Renganarayanan, *Desalination*, **173**, 77 (2005).
207. M. Khedr, *Che. Eng. Technol.*, **16**, 270 (1993).
208. I. Houcine, M. Ben Amara, A. Guizani and M. Maalej, *Desalination*, **196**, 105 (2006).
209. J. Ayoub and R. Alward, *Desalination*, **107**, 131 (1996).
210. S. Boughecha, B. Hamrouni and M. Dhahbi, *Desalination*, **183**, 151 (2005).
211. S. Abdul-Wahab, *Environ. Eng. Sci.*, **24**, 3 (2007).
212. A. Altayaran and I. Madany, *Water Res.*, **26**, 4 (1992).
213. R. Chesher, *Elsevier Oceanography Series*, **2**, 99 (1971).
214. J. Talavera and J. Ruiz, *Desalination*, **139**, 277 (2001).
215. R. Einav, K. Harussi and D. Perry, *Desalination*, **153**, 141 (2002).
216. Y. Fernández-Torquemeda, J. Sánchez-Lizaso and J. González-Correa, *Desalination*, **182**, 395 (2005).
217. J. Malfeito, J. Díaz-Caneja, M. Fariñas, Y. Fernández-Torrequemada, J. González-Correa, A. Carratalá-Giménez and J. Sánchez-Lizaso, *Desalination*, **185**, 87 (2005).
218. N. Raventos, E. Macpherson and A. García-Rubiés, *Marine Environ. Res.*, **62**, 1 (2006).
219. Y. Ruso, J. Carretero, F. Casalduero and J. Lizaso, *Marine Environ. Res.*, **64**, 492 (2007).
220. J. Sadhwani, J. Veza and C. Santana, *Desalination*, **185**, 1 (2005).
221. E. Gacia, O. Invers, M. Manzanera, E. Ballesteros and J. Romero, *Estuarine, Coastal and Shelf Science*, **72**, 579 (2007).
222. V. Manikandan, K. Shanmugasundaram, S. Shanmugan, B. Janarthanan and J. Chandrasekaran, *Renew. Sustain. Energy Rev.*, **20**, 322 (2013).
223. G. P. Narayan, M. H. Sharqawy, E. K. Summers, J. H. Lienhard, S. M. Zubair and M. A. Antar, *Renew. Sustain. Energy Rev.*, **14**, 1187 (2010).
224. A. Al-Karaghouli, D. Renne and L. Kazmerski, *Renew. Sustain. Energy Rev.*, **13**, 2397 (2009).
225. P. I. Cooper, *Sol. Energy*, **15**, 205 (1973).
226. E. S. H. Fath and S. M. Elsherbiny, *Sol. Energy*, **11**, 73 (1992).
227. K. Zhao and Y. Liu, *Desalination*, **249**, 566 (2009).
228. Z. Lu, Y. Yuan, Z. Li and Y. Zheng, *Desalination*, **298**, 22 (2012).